Opportunities and Challenges in Applying Solid-State NMR Spectroscopy in Organic Mechanochemistry

Igor d'Anciães Almeida Silva[a], Ettore Bartalucci[a,b], Carsten Bolm[c,*], and Thomas Wiegand[a,b,*]

[a] Max Planck Institute for Chemical Energy Conversion, Stiftstr. 34-36, 45470 Mülheim/Ruhr, Germany

[b] Institute of Technical and Macromolecular Chemistry, RWTH Aachen University, Worringerweg 2, 52074 Aachen, Germany

[c] Institute of Organic Chemistry, RWTH Aachen University, Landoltweg 1, 52074 Aachen, Germany

Corresponding authors: carsten.bolm@oc.rwth-aachen.de and thomas.wiegand@cec.mpg.de

Abstract

In recent years it was shown that mechanochemical strategies can be beneficial in directed conversions of organic compounds. Finding new reactions proved difficult, and due to the lack of mechanistic understanding of mechanochemical reaction events, respective efforts have mostly remained empirical. Spectroscopic techniques are crucial in shedding light on these questions. In this overview, we discuss the opportunities and challenges of solid-state nuclear magnetic resonance (NMR) spectroscopy in the field of organic mechanochemistry. After a brief discussion of the basics of high-resolution solid-state NMR under magic-angle spinning (MAS) conditions, we present seven opportunities for solid-state NMR in the field of organic mechanochemistry, ranging from *ex-situ* approaches to structurally elucidate reaction products obtained by milling to the potential and limitations of *in-situ* solid-state NMR approaches. Particular strengths of solid-state NMR, for instance in differentiating polymorphs, in NMR-crystallographic structure-determination protocols, or in detecting weak noncovalent interactions in molecular-recognition events employing proton-detected solid-state NMR experiments at fast MAS frequencies, are discussed.

Keywords: Solid-state NMR, mechanochemistry, ball milling, organic chemistry, pressure

1. Introduction

Mechanochemistry has a long track record, and historical overviews trace to back to 315 B.C.[1] The common motif is that chemical reactions are affected by mechanical forces, facilitating molecular transformations and sometimes even promoting pathways which remained unfollowed under standard reaction conditions.[2] If the mechanical energy is induced by grinding or milling, for instance by applying a ball-milling device, the term "trituration mechanochemistry" is used.[3] It has been applied on inorganic and organic compounds with scales ranging from single molecules to bulk products.[4] In recent years, more and more organic chemists started to appreciate mechanochemical techniques as they realized many attractive features including, for example, the possibility of achieving remarkable reactivities under solvent-free conditions, the option to convert insoluble substrates, the need of lower than common catalyst loading, and the observation of unprecedented products that previously had remained inaccessible.[5] In light of these advances, the recognition of the green metrics of mechanosynthesis,[6] and the scale-up opportunities by extrusion and resonant acoustic mixing (RAM),[7] industrial applications have become feasible.[8] While many of these studies focussed on the search of mechanochemical protocols for covalent bond formations, other investigations targeted supramolecular assemblies on the molecular[9] and crystalline level (polymorphs).[10] For products with new covalent bonds, common techniques for product analysis involve an aqueous work-up, followed by the use of standard organic methods (i.e. solution-state NMR and infrared (IR) spectroscopy) for the determination of the product composition and molecular structure. This contrasts the structural analyses of mechanochemically prepared supramolecular arrangements, where synchrotron powder X-ray diffraction (PXRD), Raman, and electron paramagnetic resonance (EPR) spectroscopy have been developed as *in-situ* tools (for details see below).[11] Surprisingly, the latter techniques have only seldomly been applied in the context of mechanochemical formations of purely organic products with new covalent bonds.[12]

Despite the many preparative advances and the increasing number of synthetic opportunities offered by following mechanochemical protocols, the mechanistic understanding of such processes at the molecular level has remained limited.[13] The emerging field of quantum mechanochemistry might shed light on these questions in the next future[14] although reports on ball-milling events are very rare up to date. Following the reactions, which often proceed by converting solids into solids via solids, is challenging and the use of appropriate analytical techniques are essential. The most relevant ones are briefly discussed here.

Powder X-ray diffraction[15]. PXRD is widely used for the characterization of solid materials. For mechanochemistry it is important because it gives structural information by identifying phases, purities, crystallite sizes, and morphologies.[16] As a bulk technique, it has been widely used to investigate polymorphs of co-crystals and their interconversions.[17] When studying mechanochemical reactions, the solids cannot only be analyzed *ex-situ* at the starting and the end point of the process, but also while the transformation is occurring.[18] Although such *in-situ* analyses require high-energy radiation from a synchrotron X-ray source, the effort is worthwhile because highly valuable information is obtained referencing many details of a given transformation. This is even more true for time-resolved *in-situ* (TRIS) monitoring of mechanochemical reactions, which have recently found much attention.[19] Although PXRD is very useful in studying crystallites with sizes ranging from bulk to nanoscale, it cannot provide atomic-level information. In addition, a quantification of complex multiphase materials (by Rietveld refinement) is only possible if all phase parameters of the individual components are known. Furthermore, fully amorphous material cannot be characterized, hampering the extraction of a full reaction profile.

Raman spectroscopy[20]. To analyze the progress of a mechanochemical reaction, Raman spectroscopy proved to be particularly valuable.[21] In transparent jars, this contactless method provides continuous information on the chemical composition of the reaction mixture by functional group tracking. As a consequence, a quantitative *in-situ* real-time monitoring of mechanochemical reactions is possible and kinetic models can be deduced.[22] Raman spectroscopy has also been used in combination with time-resolved *in-situ* X-ray diffraction, which allowed comprehensive analyses of molecular processes and crystalline structures.[23] The limitations of the technique are reached when the material is not Raman active or highly fluorescent. In addition, sample heating through radiation can occur, affecting the sample composition, even leading to compound degradation. Furthermore, structural details such as conformer analyses remain inaccessible.

Infrared spectroscopy. In general, IR spectroscopy is a powerful technique, which can be complementary to Raman spectroscopy. It is non-invasive and relies on interactions of infrared radiation with matter. Functional groups can be recognized providing structural information of chemical entities. With respect to mechanochemistry, manifold applications of IR spectroscopy have been reported and most of them can be classified as *ex situ*. For example, IR spectroscopy

has been used to characterize the bonding situation in non-classical *N*-metalated palladium(II) pincer complexes, which were synthesized under mechanochemical conditions. For the IR spectroscopic monitoring, aliquots of the reaction mixture were collected during the milling thereby avoiding any solubilization or other processing before the analysis.[24] Metal-free systems have also been studied by IR spectroscopy. Here, the examination of the catechol-theophylline co-crystal formation is an excellent example.[25] Directly after grinding of the two components, the samples were analyzed by attenuated total reflection (ATR) IR spectroscopy, which revealed the formation of new O–H•••O=H hydrogen bond interactions. In addition, co-crystal hydrates were determined. IR spectroscopy has also been used to evaluate the mechanochemical degradation of a pharmaceutical.[26] Thus, after milling ibuprofen in the presence of $Al(OH)_3$ for an extended period of time, degradation occurred and the resulting cleavage products were identified by various spectroscopic techniques, including FT-IR spectroscopy. Only after this initial screening (without work-up), the degradation products were extracted and isolated.[26] A related study focused on the oxidative degradation of clopidogrel hydrogensulfate, and there, ATR IR spectroscopy was used to directly analyze the crude reaction mixtures.[27] In all of the aforementioned examples, the mechanochemical processes intended to reach high conversions. However, IR spectroscopy can also be applied for analyzing mechanochemical surface modifications of solids. Along these lines, kaolinite was studied.[28] Using mid-IR and near-IR spectroscopy it was found that the mechanochemical treatment led to a destruction of the mineral surface and the loss of kaolinite hydroxyls. Concomitantly, water adsorbed on the surface.

In all presented examples, IR spectroscopy was used *ex situ*, in general, by characterizing the products after the reaction was terminated. Another approach can be followed, if gases are involved in mechanochemical reactions.[29] Those conditions allow an *in-operando* IR spectroscopy, in which the gases are passed through an outlet at the milling jar into an IR detector, where the gas composition is determined. An example of such approach was reported in the context of *in-situ* monitoring of mechanochemical reactions of hard materials.[30] There, parts of the polymeric milling device degraded, and the decomposition of the polymer was monitored by analyzing the gas phase inside the vessel. During the milling, a continuous argon flow supported the transport of the gases into the IR spectrometer, and in this manner, the formation of CO, CO_2, water, and hydrocarbons was evidenced.

EPR spectroscopy[31]. This technique detects unpaired electrons and allows investigation of the structure and bonding situation of paramagnetic species. It is highly sensitive, requiring only μM concentrations, and has an extraordinary time resolution in the range of ns. Multiple applications have been reported in the context of mechanochemistry. Many of them involve the detection of paramagnetic metals in an environment resulting from a mechanochemical synthesis of a particular material.[32] Others focus on the generation of radicals by grinding of solids such as quartz sand, for example.[33] In related work, EPR spectroscopy was used to demonstrate the occurrence of mechanochemically-induced solid-state single electron transfer by grinding of dipyridinium cations in stainless-steel milling devices.[34] Mechanochemical conversions of soft materials including polymers have also been studied by EPR spectroscopy. For example, oxygen- and carbon-centered radicals were detected in the mechanochemical depolymerization of polystyrene.[35] Furthermore, mechanophores forming radicals reversibly have been incorporated into polymeric systems, and their freezing-induced mechanochemistry has been studied by EPR spectroscopy.[36] Finally, spin labels have been applied. For example, after grafting stable nitroxyl radicals by solid-phase mechanochemistry on cellulose, EPR spectroscopy revealed the presence of two types of "isolated" radicals and it was possible to investigate exchange interactions between neighbouring spins in the crystal.[37] While the sensitivity of EPR spectroscopy is very appealing, it remains an *ex-situ* technique. Thus, the radicals will be detected before or after the mechanochemical treatment, which might also involve the introduction of spin traps. To the best of our knowledge, *in-situ* EPR studies proceeding under mechanochemical conditions have remained unreported.

Miscellaneous. Due to the analytical challenges associated with the hard materials of the milling device (for example, tungsten carbide, stainless-steel, zirconia, or agate) and the mostly demanding mechanochemical reaction conditions, *in-situ* and *in-operando* monitoring is difficult. In recent years, however, technical advances have improved the situation, and now, milling devices with sensors of temperature and pressure changes are available. Those parameters can then also be used for following and analyzing mechanochemical processes. Two examples shall illustrate these approaches here. In the first one, a mechanochemically induced benzil-benzilic acid rearrangement was studied.[12] Besides synchrotron powder X-ray diffraction and Raman spectroscopy, real-time temperature sensing was used to visualize the ongoing molecular migration. Although the temperature changes were only small (1-2 °C), they could be well detected, and they confirmed the timing of the rearrangement in accord to the results previously obtained by analyzing the PXRD pattern. In the second example, a

mechanochemical carbonylation reaction was monitored by using a pressure sensor.[38] With metal hexacarbonyl complexes as CO source, most combinations with K_3PO_4 as base led to a pressure increase indicating the formation of gaseous CO. This result contrasted the one observed with the optimized palladium catalyst system, where such pressure increase did not occur, suggesting a fast CO transfer from the metal hexacarbonyl complex to the active palladium species, which then carbonylated the substrate leading to product formation. Thus, in this case, a clear mechanistic hint could be deduced by using this advanced monitoring device.

Without doubt, each of the aforementioned analytical methods has significantly advanced the understanding of the underlying principles of mechanochemical processes. Following the reactions by spectroscopical means while they proceed (*in-operando*) and even inside their natural reaction environment (*in-situ*) allows to gain major experimental insight, which expands our fundamental knowledge and even more so is important for further directed discoveries in mechanochemistry. Surprisingly, however, one important tool that organic chemists very commonly used for analyzing product mixtures and determining molecular structure is underrepresented in mechanochemistry: NMR spectroscopy. Surely, it is a common tool for characterizing the final outcome of the reaction by measuring the crude or purified products. That, however, is mostly done by solution studies, which involves a dissolution of the products, with the danger of altering their composition. But why is that so and how about a direct analysis of the solid product mixture? Solid-state NMR spectroscopy is offering that option. Without dissolving the sample, the analysis can be performed providing valuable information on product composition and structure. The current state-of-the-art, the potential future opportunities, and the challenges in applying solid-state NMR in organic mechanochemistry are discussed here.[39]

2. Main part

2.1. High-resolution solid-state NMR spectra achieved by magic-angle spinning

Solid-state NMR has developed into a versatile tool for studying structures and dynamics in several disciplines, comprising materials sciences, pharmaceutics and biology. In contrast to NMR in solution, a solid sample contains a huge number of crystallites, each of which can be oriented in a powdered sample with a certain angle θ with respect to the external magnetic field, typically denoted with B_0. The NMR interactions, such as the chemical shift or dipolar coupling between nuclei, depend on this angle θ, in most cases via the second-order Legendre polynomial $(3cos^2\theta - 1)$, which renders such interactions anisotropic. Therefore, in a powdered sample, in which all crystallite orientations appear according to their statistical probability, different resonance frequencies for the individual spins with different orientations are expected. Figure 1 illustrates this for the example of the chemical-shift anisotropy: Each crystallite orientation leads to a different resonance frequency, thus leading to broad NMR resonances, the so-called static "powder line shape". In solution, however, such anisotropic interactions are typically averaged out by the highly efficient Brownian molecular-motion process, such that only the isotropic part of an NMR observable can be observed (*e.g.,* the isotropic chemical-shift, δ_{iso}, or the isotropic *J*-coupling constant, J_{iso}). In cases where several chemically-equivalent species are present in the powdered sample, the static solid-state NMR spectrum becomes often featureless and uninterpretable.

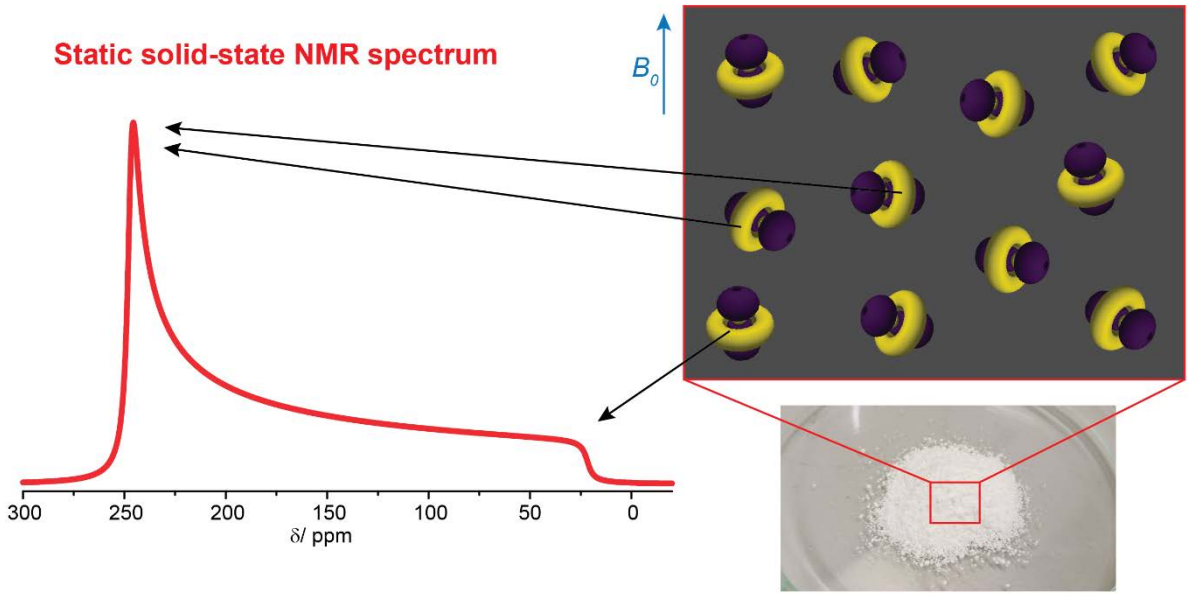

Figure 1: Anisotropic interactions yield to broad static solid-state NMR spectra. Example of a static ^{13}C powder line shape dominated by chemical-shift anisotropy. The powder consists of various crystallites with different orientations with respect to the external magnetic field schematically represented by spherical tensors.

A closer look at the angle-dependence of the second-order Legendre polynomial reveals that this expression becomes zero at an angle of θ~54.74°, which means that crystallites possessing this specific orientation with respect to B_0 should not be affected by the anisotropic interaction and should resonate at δ_{iso}, the same chemical-shift value they would possess in solution. The question to be answered is, thus, if it is possible to align all crystallites of a solid sample- on time average- along that angle of 54.74° with respect to B_0?

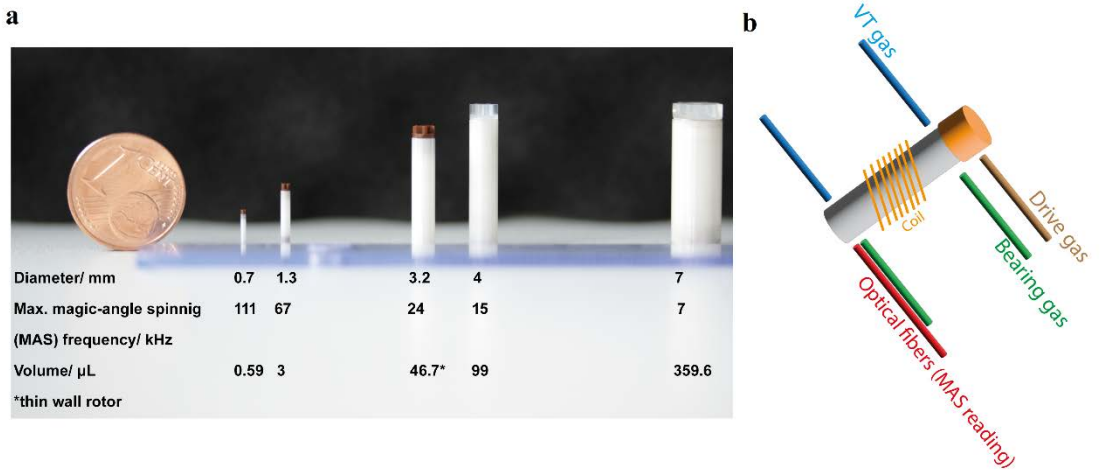

Figure 2: a Five routinely used MAS NMR rotors with 0.7 mm, 1.3 mm, 3.2 mm, 4.0 mm, and 7.0 mm outer diameters (left to right) compared with a 1-cent Euro coin. Several rotor characteristics, such as maximum MAS frequency and rotor volume are reported. The Figure has been prepared by Dr. Boran Uluca-Yazgi and Dr. Rıza Dervişoğlu (both MPI CEC). **b** Schematic drawing of a solid-state NMR stator used for spinning a cylindrical NMR rotor.

The technique exactly fulfilling this requirement is called magic-angle spinning (MAS)[40] – a "magic" technique, since it averages anisotropic interactions and produces high-resolution NMR spectra. For an MAS experiment, the solid sample is packed in cylindrical sample containers (the NMR rotors), typically made from ZrO_2, a material possessing one of the highest harnesses and flexural strengths. The rotor is sealed by a cap having the form of a turbine (see Figure 2), typically made from the polymer VESPEL. The central idea of the MAS experiment is to rotate the MAS rotor with several kHz around an axis, which is inclined by the magic angle (54.74°) with respect to the magnetic field. For that purpose, two airflows are employed, one directed on the rotor cap (the drive gas) and the other lifting the rotor in the NMR stator (the bearing gas), see Figure 2b for a schematic representation. The maximal available MAS frequency is determined by the outer diameter of the NMR rotors: The smaller such rotors become, the faster they can spin. Figure 2 shows five routinely applied MAS rotors

with outer diameters of 7.0 mm, 4 mm, 3.2 mm, 1.3 mm and 0.7 mm, in which maximal MAS frequencies of 7 kHz, 17 kHz, 24 kHz, 66 kHz and 111 kHz, respectively, can be achieved. As a matter of fact, the smaller such rotors become, the less material can be packed therein, in case of the 0.7 mm rotor only sub-milligram of sample amounts can be used. The record in achieved MAS frequencies is 170 kHz in these days, employing rotors with an outer diameter of 0.5 mm.[41] Note, that also spherical rotors have been described recently.[42] Fast MAS frequencies are mandatory for obtaining high-resolution proton spectra, since the proton-proton dipolar couplings are not sufficiently averaged at low MAS frequencies (<60 kHz), leading, in general, to unresolved spectra.[43] Also in case of paramagnetic materials, where short relaxation times and large anisotropic interactions hamper their analysis, fast MAS is a convenient tool to overcome such limitations.[44]

MAS affects the spun sample in three ways. (i) Frictional heating between the rotor and the gas used for MAS (typically pressurized air) increases the sample temperature. For instance, rotating a 3.2 mm rotor at 20 kHz increases the sample temperature by around 25 K,[45] which, however, can be compensated by actively cooling the sample. (ii) The centrifugal gravitational forces acting on the sample induce accelerations in the order of several 10^6 *g*, in case of MAS experiments performed at 111 kHz in 0.7 mm rotors around $12 \cdot 10^6$ *g* (typical accelerations in the ultracentrifuge are around 10^5 *g*).[45] (iii) The centrifugal forces induce centrifugal pressure, which reaches its maximum on the inner rotor wall (for more details see Section 2.3).

Although MAS averages out anisotropic NMR interactions, it might be necessary to recouple them again under MAS to explore their full potential in NMR-based structure determinations. For instance, recoupling of the dipolar interactions (*e.g.* between heteronuclei) enables the determination of internuclear distances. A prominent example is the Rotational Echo Double Resonance (REDOR) experiment[46] that has been used in a broad range of applications.

2.2 Current limitations and challenges of high-resolution solid-state NMR spectra in organic mechanochemistry

In-situ analytical tools are of high importance to develop a mechanistic understanding of organic mechanochemical transformations. For static solid-state NMR, an *in-situ* approach was already reported,[47] where a vibrational ball mill was integrated into a modified static solid-state NMR probe (Figure 3). The authors employed an electric stepper motor located outside of the stray field of the magnet and a transmission system to effectively mimic a vibrational ball

mill. The system was built in order to allow translational displacements of up to 1.0 cm and, during this movement, the reaction vessel/sample container is kept inside the radio frequency-coil. With this modified probe, the formation of zinc phenylphosphonate from zinc acetate and phenylphosphoric acid was followed by real-time static NMR measurements. As a matter of fact, a similar modification of an MAS NMR probe does not appear to be feasible since, for instance, the translational motion that would mimic the shaking of the ball mill would interfere with the rotation of the sample around the magic angle as required to achieve high-resolution solid-state NMR spectra. Whether for instance the centrifugal pressures acting during MAS are already sufficient to induce organic mechanochemical reactions will be discussed in detail in Opportunity 5.

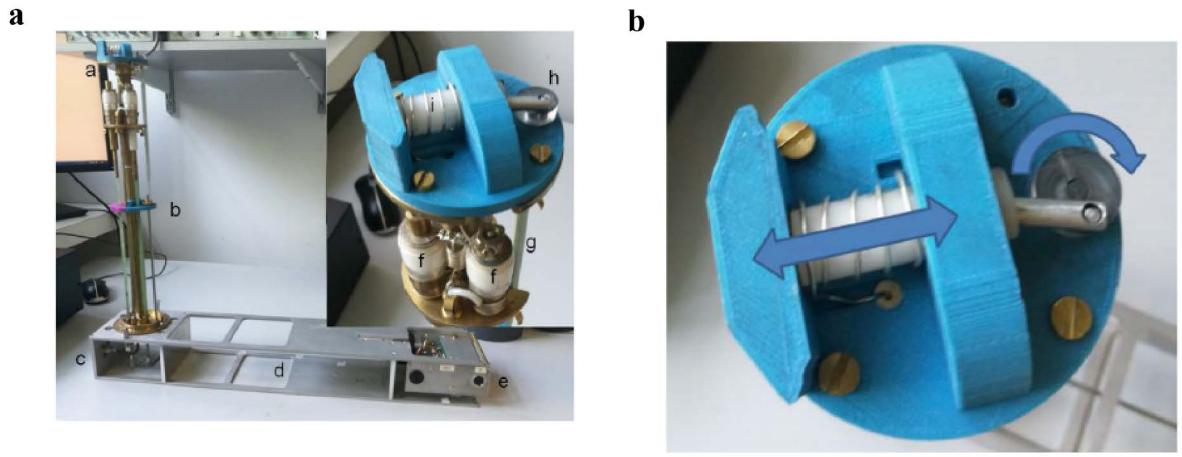

Figure 3: a Integration of a vibrational ball mill into a static solid-state NMR probe. The inset shows the top part of the probe with the ball-milling device; **b** Top part of the probe with indication of motions; All colored parts were 3D printed using polylactic acid (PLA). Reproduced with permission from reference [47].

2.3 Opportunities of high-resolution solid-state NMR spectra

Opportunity 1: Studying milling reaction products by ex-situ solid-state NMR without further post-processing

A particular strength of solid-state NMR is that it directly enables the investigation of the solid material taken from the milling jar, requiring no further post-processing. NMR itself is a non-destructive technique and allows for an element-selective analysis on the atomic level, thus being sensitive to smallest local structural changes, which, for instance, directly affect the NMR chemical-shift values. Typical nuclei that can be studied by solid-state NMR in the context of organic mechanochemistry are ^{1}H, ^{13}C, ^{15}N, ^{19}F and ^{31}P, in all cases requiring MAS (see Section 2.1) to obtain high-resolution NMR spectra. The low natural abundance combined with the small gyromagnetic ratio, γ_I, of ^{13}C and ^{15}N lead to a rather poor signal-to-noise ratio

(SNR) in the NMR experiment for such nuclei (the SNR is proportional to $\gamma_I^{5/2}$). The cross-polarization (CP) experiment, in which the polarization from the more abundant ^{1}H nuclei is transferred to the ^{13}C and ^{15}N nuclei, improves the SNR theoretically by a factor of four for ^{13}C and a factor of ten for ^{15}N and allows using shorter repetition times. Such CP spectra, however, are *a priori* not quantitative (*vide infra*). ^{1}H- and ^{19}F-detected experiments require fast MAS frequencies (> 60 kHz, see above) to efficiently average the homonuclear dipolar coupling interactions.[43, 48] Figure 4 shows a representative characterization of a cyclic sulfoximine employed in organic mechanosynthesis (*vide infra*) by 2D ^{1}H,^{13}C hCH correlation, ^{13}C,^{1}H CP-MAS (projection on the 2D spectrum in the indirect dimension in Figure 4b), 2D ^{1}H-^{1}H spin-diffusion, as well as ^{15}N,^{1}H CP-MAS spectra.

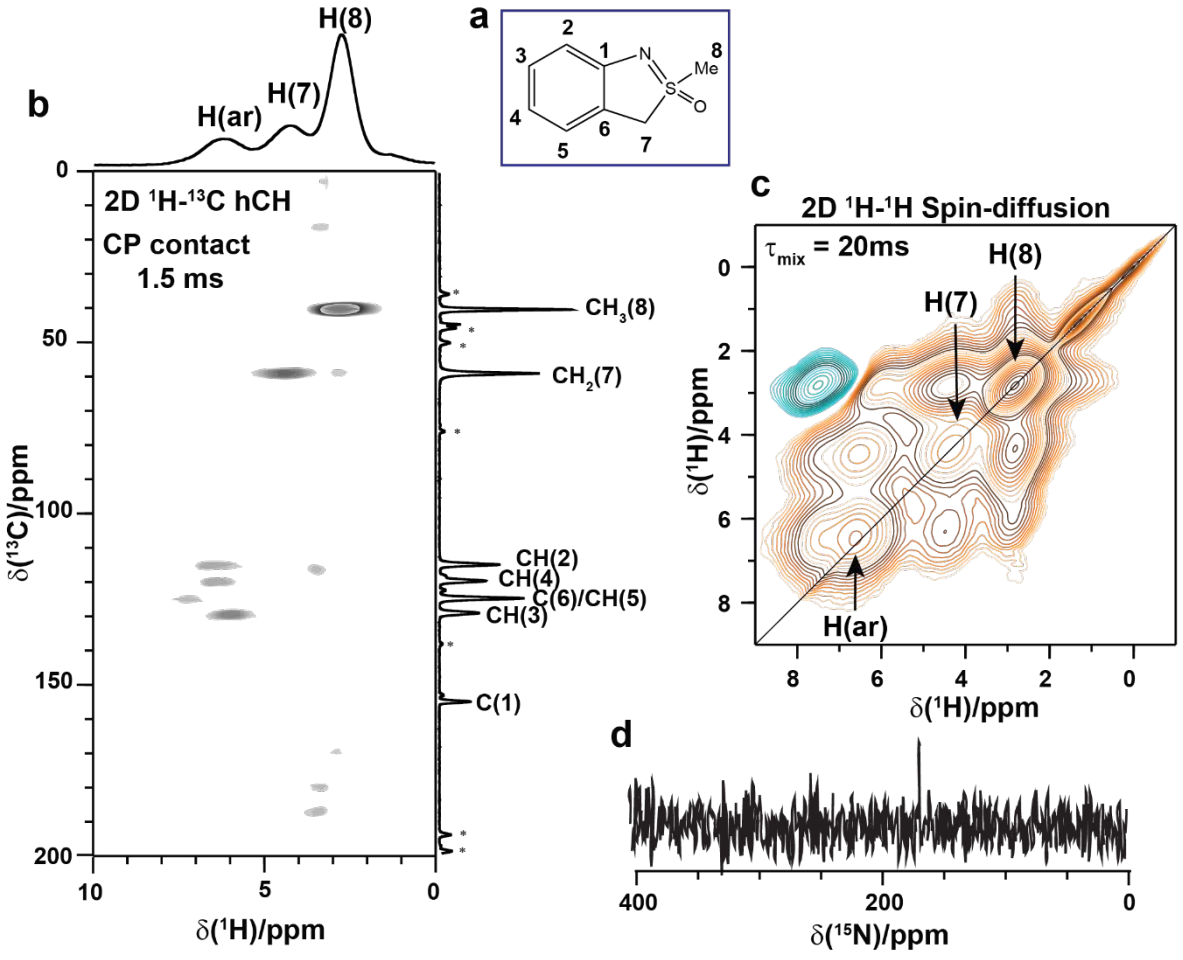

Figure 4: Structural characterization of a cyclic sulfoximine used in organic mechanosynthesis. **a** Chemical structure of the starting material, **b** 2D hCH correlation spectrum including the 1D ^{1}H MAS and ^{13}C,^{1}H CP-MAS spectra as projections on the 2D spectrum. The ^{1}H-detected spectra have been recorded at 60 kHz MAS. **c** 2D ^{1}H-^{1}H spin-diffusion based spectrum and **d** ^{15}N,^{1}H CP-MAS spectrum. Reproduced from reference [49] under CC BY-NC-ND 4.0 license (https://creativecommons.org/licenses/by-nc-nd/4.0/).

In that vein, solid-state NMR is a powerful method in *ex-situ* characterization of ball-milling products, in which even kinetic information are accessible by recording spectra on the solid mixture taken from a ball mill in discrete time steps. This has, for example, been applied to study the mechanochemical synthesis of alane, AlH_3[50] and to characterize the mechanochemical properties of $LiBH_4$:$AlCl_3$ mixtures.[51] We recently studied the bromination of a cyclic sulfoximine (more specifically 2-methyl-3*H*-2λ^4-benzo[*c*]isothiazole 2-oxide, **1**) with *N*-bromosuccinimide (NBS, **2**) to give a brominated sulfoximine (**3**) and succinimide (**4**) in a mixer ball mill and used solid-state NMR to access the reaction time until full conversion of the starting materials was achieved (for the chemical reaction see Figure 5). Figure 5 shows the ^{13}C,^{1}H CP-MAS spectra of the solid material taken from the ball mill at different time points. Apparently, tiny-resonances for starting material **1** are still present in the first spectra (after 5 and 15 min of ball milling), and full conversion was observed after 30 min.

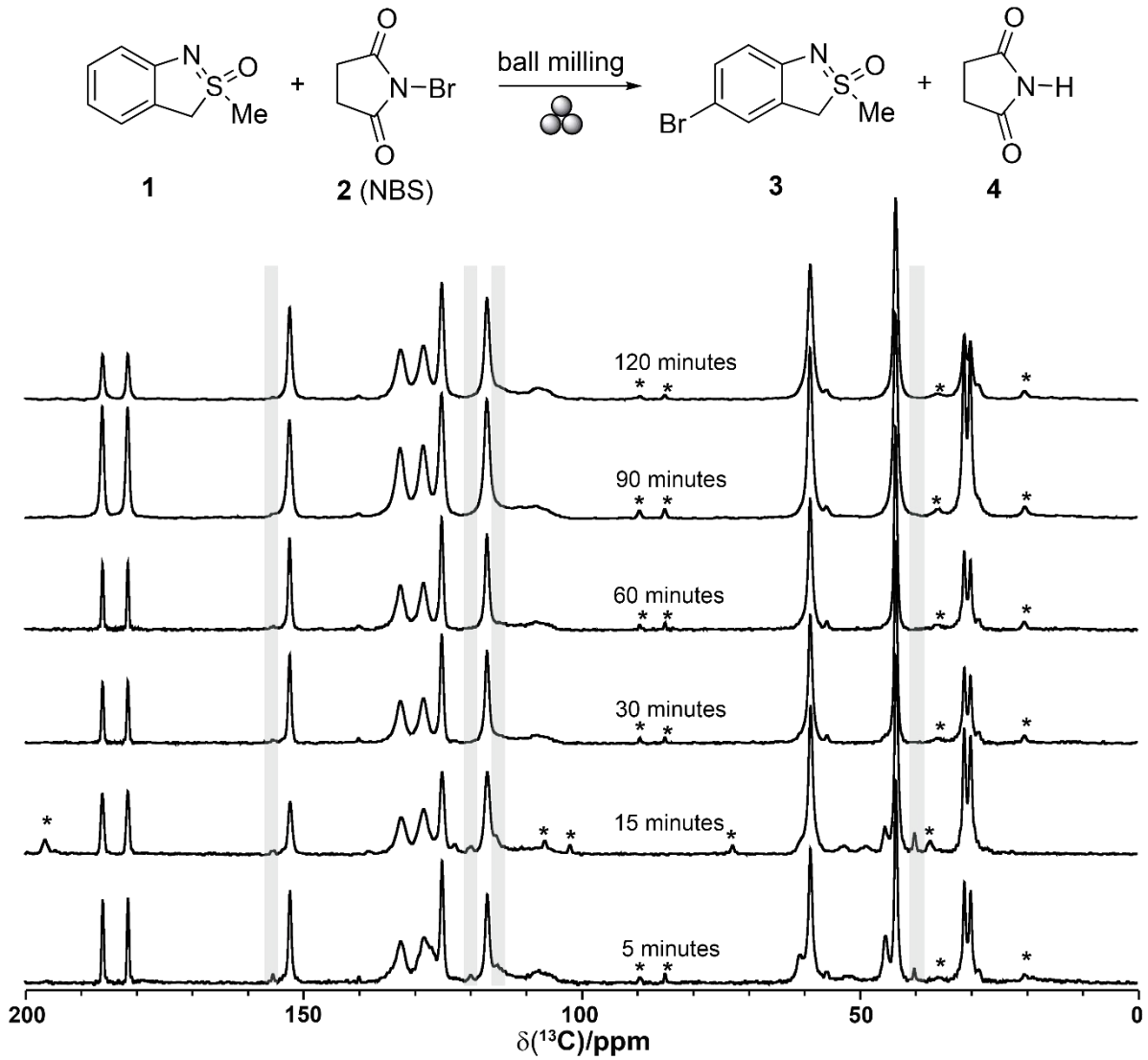

Figure 5: ^{13}C,^{1}H CP-MAS spectra of samples taken at discrete time points from the milling jar for the bromination reaction of a cyclic sulfoximine (for the reaction scheme see top of the figure). The resonances highlighted in grey are assigned to the sulfoximine starting material. Full conversion is observed after 30 min of ball milling. * indicates MAS sidebands. Reproduced from reference [49] under CC BY-NC-ND 4.0 license (https://creativecommons.org/licenses/by-nc-nd/4.0/).

Ex-situ phosphorus-31 MAS NMR experiments have been for instance applied to elucidate the reaction products of the Wittig reaction,[52] to study the mechanochemical formation of phosphonium salts by milling triphenylphosphine with solid organic bromides,[53] and to characterize two Pt-complexes [*cis*-$(Ph_3P)_2PtCl_2$ and *cis*-$(Ph_3P)_2PtCO_3$)] formed upon milling polycrystalline $PtCl_2$ with Ph_3P, and *cis*-$(Ph_3P)_2PtCl_2$ with an excess of anhydrous K_2CO_3, respectively.[53] In most cases, the spectra from the reaction products formed in the milling jar are compared to their crystalline analogues and identical NMR spectral fingerprints serve as a proof for successful product formation. ^{13}C solid-state NMR has been, for instance, explored to develop an understanding of C-N amide bond formation using the coupling reagent *N*-(3-(dimethylamino)propyl)-*N*′-ethylcarbodiimide hydrochloride, in which an intermediate of its reaction with benzoic acid has been isolated and characterized.[54]

Advantageously, solid-state NMR can also detect the formation of amorphous phases, which sometimes escapes powder XRD by just appearing as a broad background in the powder pattern (*vide infra*).[53] An attractive approach in structural characterization of milling products is the combination of the atomic-level information encoded in solid-state NMR spectra, where each resonance is a sensitive probe for the local structure, with the powder XRD pattern reporting on the space group of the crystalline material ("NMR crystallography", see also opportunity 2). Tracing back spectral changes occurring upon milling-induced product formation for all atoms is a further advantage of solid-state NMR, for instance compared to Raman and IR spectra, in which only certain functional groups are unambiguously identified.

Finally, there is another important aspect: *Ex-situ* solid-state NMR allows the direct analysis of the product composition obtained by the mechanochemical process. This contrasts the product characterization by solution-state NMR, which often involves a work-up or at least requires the dissolution of the products in the NMR solvent. Both of these dissolution steps can lead to unwanted reactions and alter the product composition. These changes can be excluded by the use of *ex-situ* solid-state NMR. An illustrative example is the formation of a unique polymorph of Wilkinson's catalyst by ball milling.[74] Immediately after its mechanochemical formation it was characterized by solid-state NMR. An analysis by solution-based NMR would

have been impossible due to the loss of polymorphic structural information caused by the dissolution.

Another example demonstrating the high value of *ex-situ* solid-state NMR stems from a study with *a*-(trifluoromethyl)-lactic acid (TFL).[16] This compound is known for its unusually high sublimation tendency, which can lead to a rapid alternation in the enantiomer composition of a scalemic sample.[55] Direct analyses of TFL mixtures by *ex-situ* solid-state NMR provides reliable data, since the optical pure phases can be distinguished from the racemic compound,[56] whereas solution-based NMR techniques cannot differentiate between those phases and come with the danger of losing parts of the product by sublimation, thereby changing the enantiomer ratio of the sample to be analyzed.

In fact, *ex-situ* applications of solid-state NMR are not only limited to the study of milling processes, but have also been explored in the context of extrusion setups. For instance, ^{13}C-detected solid-state NMR has revealed the successful preparation of a series of *N*-acylhydrazones via twin-screw extrusion.[57]

Opportunity 2: Structure determination of reaction products by NMR crystallography

One of the strengths of mechanochemistry is the possibility to synthesize new crystalline materials (or polymorphs, *vide infra*) not accessible by other synthetic routes. Therefore, structure determination is essential to characterize these materials, particularly to compare their structures to those obtained by "conventional" synthesis routes in solution. While single crystal-ray diffraction is certainly the method-of-choice in determining the structures of organic compounds, growing single crystals from the material obtained in a mechanochemical milling reaction would require dissolving the compound in a suitable crystallization solvent, eventually giving a false result on the outcome of the reaction. "NMR crystallography" has developed into an important tool in structure determination and has been applied to a variety of material classes, comprising for instance small organic molecules, pharmaceutics or supramolecular assemblies.[58] NMR crystallography combines the advantages of NMR (for instance in localizing hydrogen atoms possessing a low X-ray scattering factor or distinguishing isoelectronic species) and powder X-ray diffraction, allowing for instance the initial structure determination via Rietveld refinement supplemented with simulated annealing approaches.[59] Structural inputs and constraints (or restraints) from solid-state NMR are used in an iterative structure-determination protocol to refine the XRD structural model (note that NMR inputs might also been used only in validating the structures obtained from potentially ambiguous

diffraction data). This process is supported by density functional theory (DFT) calculations, particularly of NMR observables, which are feasible with rather high accuracy for solids using Gauge Including Projector Augmented Waves (GIPAW)[60] implemented in several quantum-chemistry software packages.[61]

The wealth of information encoded in NMR spectra are employed in NMR crystallography. To outline a few: The number of crystallographically distinct molecules in the asymmetric unit of the crystal can be deduced from the number of NMR signals for a specific atom, since NMR chemical-shift values are highly sensitive reporters on the smallest structural differences.[62] Hydrogen atoms can be positioned very accurately, for instance by exploring the ^{1}H chemical shift, which reacts highly sensitive to noncovalent interactions (see also opportunity 7). The packing of molecules can be unravelled by probing intermolecular interactions, using either *J*-coupling (via chemical bonds) or dipolar-coupling (through-space) based NMR techniques. Such experiments are of high importance for instance in proving co-crystal formation (*vide infra*).

NMR crystallography has been employed already in the field of mechanochemistry, for instance in structure determination of organic mechanochemical products like multi-component crystals containing urea,[63] fluoxetine HCl co-crystals,[64] and Zn-Terephthalate networks.[65] In these examples, solid-state NMR on quadrupolar nuclei (^{17}O and ^{35}Cl) was employed. DFT-calculated electric-field gradient (EFG) tensors were explored from an initial structure model based on the powder X-ray diffraction pattern data and refined using the solid-state NMR data gathered for the studied crystals. For multi-component crystals containing urea, experimental ^{35}Cl EFG tensors were used as a figure of merit for further refinement of the crystal structure. First, the reported crystal structures of the multi-component crystals (based solely on X-ray diffraction data) were used to predict the EFG tensors, leading to a not perfect correlation between experimental and calculated EFG tensor. Then, these structural models were refined using plane-wave DFT showing a much better correlation.

Opportunity 3: Distinction of crystalline and amorphous phases and direct analysis of the longitudinal relaxation times as a measure for particle sizes

a) Distinction of crystalline and amorphous phases by changes in NMR linewidths

The lack of crystallinity is often associated with a broadening of solid-state NMR resonances (denoted as a heterogeneous broadening of the NMR resonances) caused by a distribution of chemical-shift values originating from structural disorder. It is reported for several examples that subjecting a crystalline material to ball milling for several hours induces

the formation of amorphous phases,[66] for which consequently broad solid-state NMR resonances would be expected. This has been for instance observed in milling crystalline trehalose[67] (see Figure 6) or crystalline platinum-complexes.[53]

Note that entire amorphous materials escape powder XRD detection, but they still appear as broad features in solid-state NMR spectra. Also, gel-type materials are highly suitable for solid-state NMR, as particular studies on microgels, hydrogels and proteins reveal.[68]

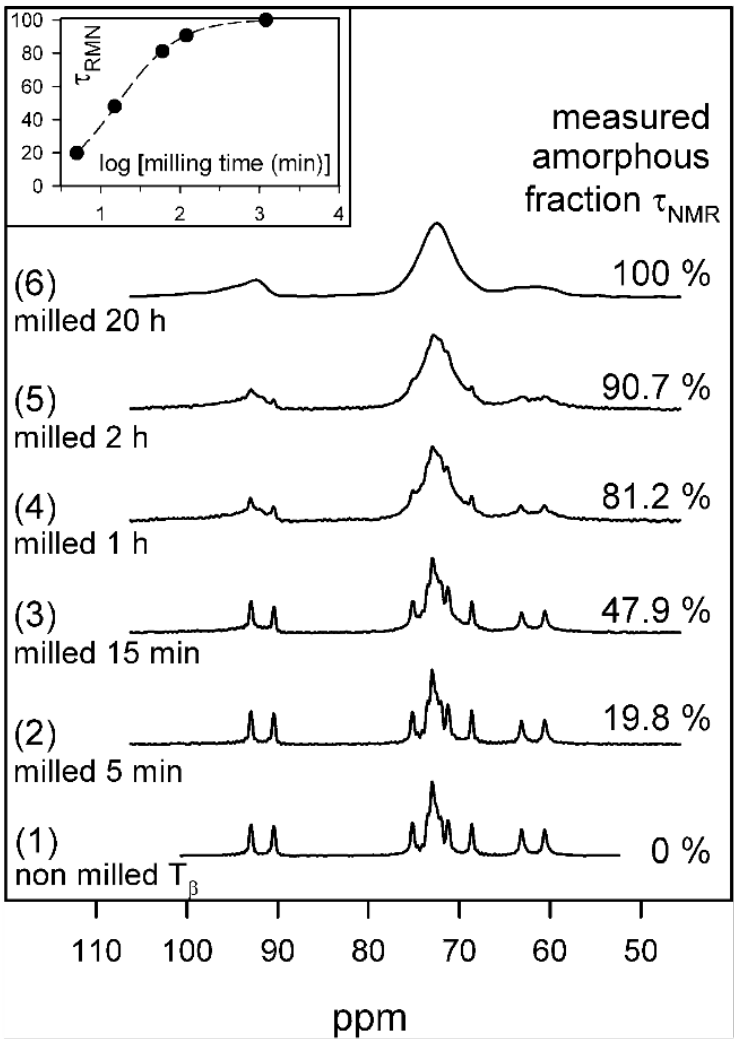

Figure 6: ^{13}C MAS spectra of trehalose subjected to different times of ball milling. The amorphous fraction is determined from the NMR spectra and reported on the right of the individual spectra. Reproduced with permission from reference [67].

b) Proton longitudinal relaxation times as a probe for changes in particle sizes upon milling.

Longitudinal relaxation times measured by solid-state NMR have been explored intensively, for instance in the field of polymer chemistry, to report on changes in sample crystallinity.[69] Amorphous phases typically possess shorter relaxation times than crystalline

ones, typically associated with higher mobility in the amorphous phases. It has been reported that ball milling initially leads to smaller particle sizes, whereas upon long milling times also the formation of amorphous phases has been observed.[67] For instance, ball milling of trehalose for 20 h gives a fully amorphous phase as indicated by broadened ^{13}C solid-state NMR resonances (see Figure 6), as well as changes in the melting behaviour monitored by Differential Scanning Calorimetry (DSC).[67]

While the width of reflexes in powder XRD spectra directly encodes information about crystallite sizes (the so-called Scherrer equation), this information cannot be directly extracted from NMR linewidths (although qualitative correlations between decreasing particle sizes and increasing NMR linewidths have been reported in some cases, such as for metal phosphide nanoparticles in which resonance broadening is caused by alterations in surface-electron states[70]). However, ^{1}H longitudinal relaxation times have been shown to correlate with particle sizes. For instance, the pharmaceutic dicumarol has been subjected to cryo-grinding and indeed, a correlation between the particle size determined by scanning electron microscopy (SEM) and longitudinal relaxation times has been found.[71] The smaller the particles, the shorter the ^{1}H longitudinal relaxation time, which has been associated with crystal defects serving as relaxation sinks.[71] Similar observations and conclusions have been drawn for crystalline α-lactose monohydrate[72], as well as Gabapentin.[73]

We have observed the same features in studying the discussed bromination of a cyclic sulfoximine cited in *Opportunity 1*, in which succinimide is formed as a by-product. Purchased succinimide is highly crystalline and possesses a ^{1}H T_1 relaxation time of > 3500 s (see Figure 7a), which shortens by two orders of magnitude after 1 h of ball milling (Figure 7b). The ^{13}C CP-MAS spectra, however, do not show any substantial peak broadening pointing to the absence of a significant amount of amorphous phase (Figure 7c, note that the MAS frequencies are different and thus the ^{1}H decoupling schemes differ). In fact, we believe that the formation of an amorphous phase has relevance for organic mechanosynthesis in general and that it might, for example, explain the observation of an induction period (for an example see ref [19b]) in which no transformation occurs, but particle sizes decrease (as reported by time resolved X-ray diffraction[19a]) and tiny amounts of amorphous, highly mobile phases, are formed.

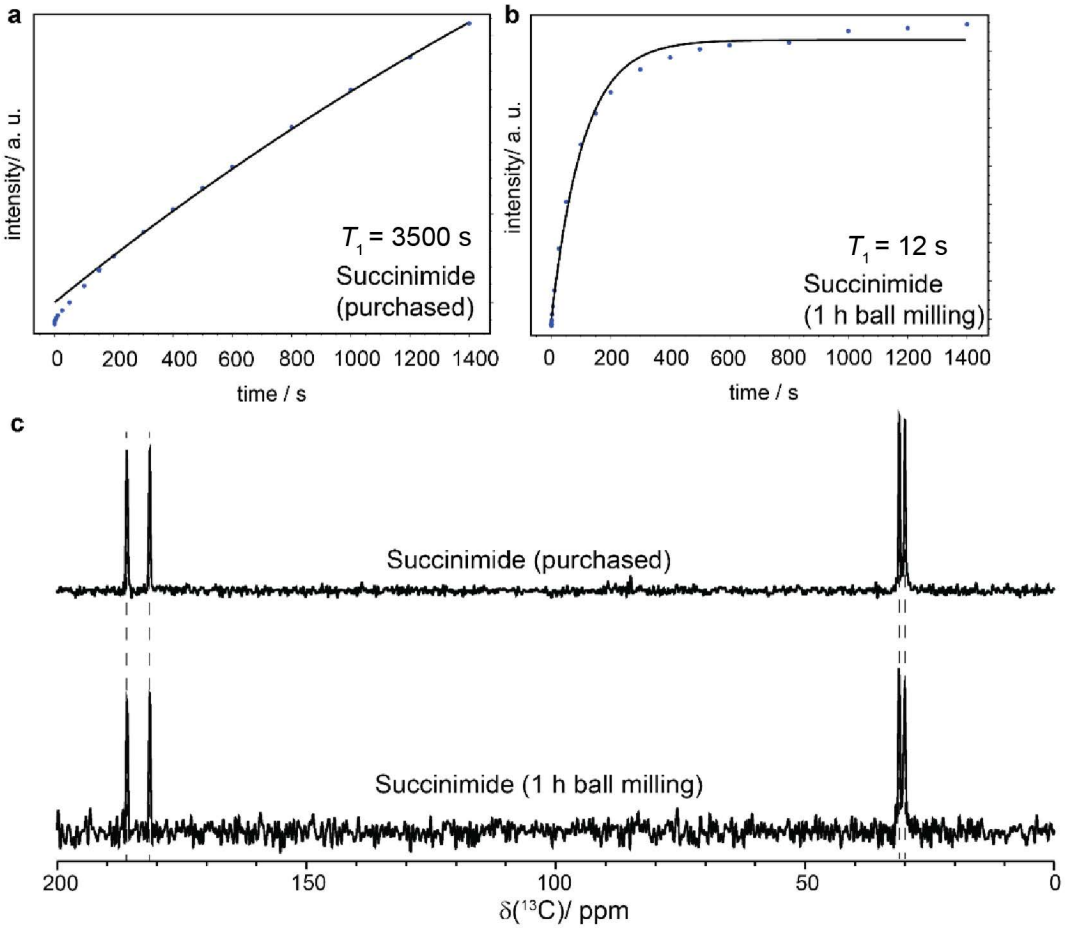

Figure 7: Comparison between ^{1}H longitudinal relaxation times (T_1) of purchased succinimide (**a**) and ground succinimide after 1 hour of ball milling (**b**) obtained by saturation recovery experiments performed at 60 kHz and 16.4 T static magnetic field. **c** ^{13}C CP-MAS spectra of both purchased (top) and ground (bottom) succinimide recorded at 17 kHz (top) and 60 kHz MAS (bottom) at 16.4 T static magnetic-field strength. Adapted from reference [49] under CC BY-NC-ND 4.0 license (https://creativecommons.org/licenses/by-nc-nd/4.0/).

Opportunity 4: Identification of polymorphs

Mechanochemistry is a highly efficient technique to synthesize and screen polymorphs of organic solids,[74] which is a key factor for pharmaceutical research, since different polymorphs exhibit different physicochemical properties due to different crystal structures.[17b, 75] Therefore, it is necessary to have spectroscopic techniques available allowing for a simple differentiation of these polymorphs. X-Ray Diffraction (XRD) is extensively used for both *ex-situ* and *in-situ* distinction of polymorphs,[17c, 74b, 76] but also solid-state NMR can be used to this end. Several NMR observables, such as chemical-shift values, can be affected by different chemical environments present in the polymorphic solid-state structures. For instance, ^{13}C CP-MAS can be used to identify *in-situ* transient polymorphism during the crystallization of glycine

in different solvents, since the different polymorphs of glycine exhibit different ^{13}C chemical shift-values for the carbonyl group.[77] Another example of NMR observables that can be affected by polymorphism are static line shapes and spin-lattice relaxation time (T_1), which can be affected by the differences in bond geometries and crystal packing.[78] Although the use of solid-state NMR for identifying different polymorphs is straightforward, examples from organic mechanochemistry are scarce in the literature.

As referred to under *Opportunity 1*, ^{31}P MAS NMR was able to differentiate the two polymorphs of the Wilkinson's catalyst (WC) [$RuCl(PPh_3)_3$],[79] which showed different catalytic activities in hydrogenation reactions performed upon ball-milling conditions. Orange WC was prepared by ball-milling rhodium(II) chloride hydrate and PPh_3 at 25 Hz for 90 minutes. Figure 8 displays both ^{31}P MAS NMR spectra and powder XRD pattern of both polymorphs (red and orange) as well as the spectrum for the sample prepared by liquid assisted grinding (LAG). As one can see, both solid-state NMR and powder XRD were able to show that LAG favoured the orange polymorph.

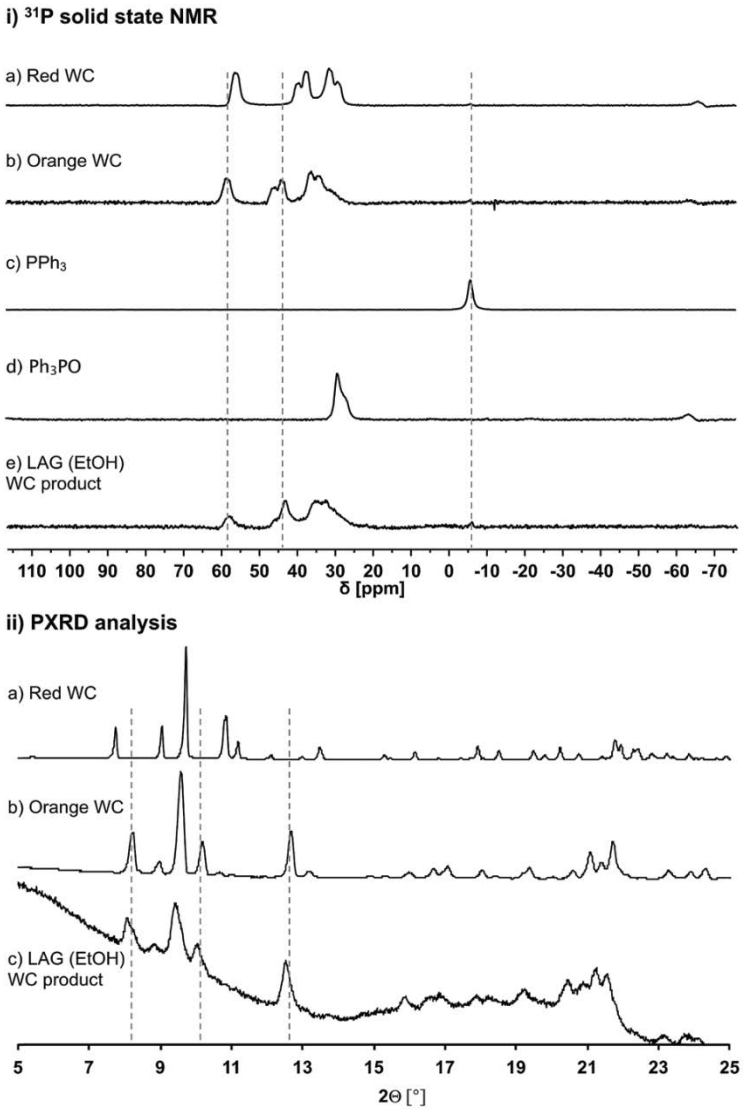

Figure 8: ^{31}P MAS NMR spectra (i) and powder XRD (ii) pattern of both polymorphs of Wilkinson's catalyst (red and orange, respectively) prepared without and with ball milling. Upon ball milling, the NMR spectra indicate that the orange polymorph is formed. NMR spectra of PPh_3 and Ph_3PO are additionally shown. Reproduced with permission from reference [79].

In another work, the differentiation of polymorphs of co-crystals of pyrazinamide (PZA) with malonic acid (MA) formed upon grinding was achieved by ^{1}H-detected MAS NMR.[80] Spectral changes observed for the co-crystal phases with respect to the individual crystalline phases clearly allowed concluding on successful co-crystal formation. It was even possible to distinguish different polymorphs based on their characteristic signatures in ^{1}H MAS spectra pinpointing again to the high sensitivity of the NMR chemical-shift values (see Figure 9).

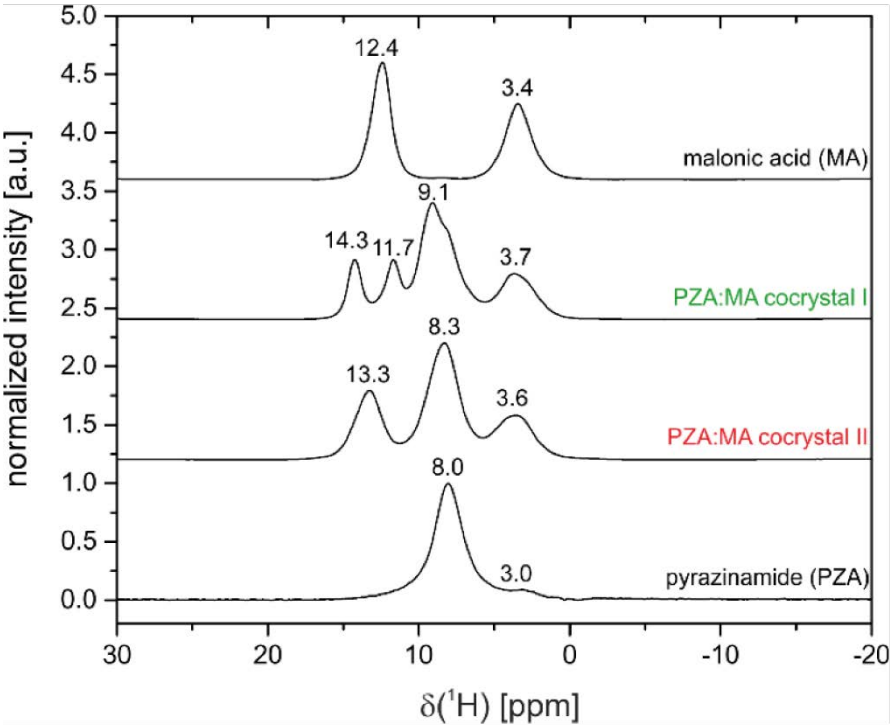

Figure 9: ^{1}H MAS spectra recorded at 25 kHz MAS and at a magnetic field of 14.1 T of crystalline pyrazinamide and malonic acid (black), as well as two co-crystalline phases (red and green). Reproduced with permission from reference [80].

Solid-state NMR has also been successfully applied to distinguish pseudo-polymorphs, which arise upon embedding solvent molecules within the crystalline lattice. The high sensitivity of NMR observables allows a straightforward distinction of such species. Figure 10 illustrates this concept for the example of a *P*,*P*-[3]ferrocenophane, for which ^{31}P MAS spectra allowed a clear distinction of the three polymorphic phases based on different chemical-shift values, as well as *J*-coupling constants.[81] In case of polymorph A, dichloromethane is incorporated in the crystal structure and the asymmetric unit contains two crystallographically-distinct molecules (denoted with A and A' in Figure 10).

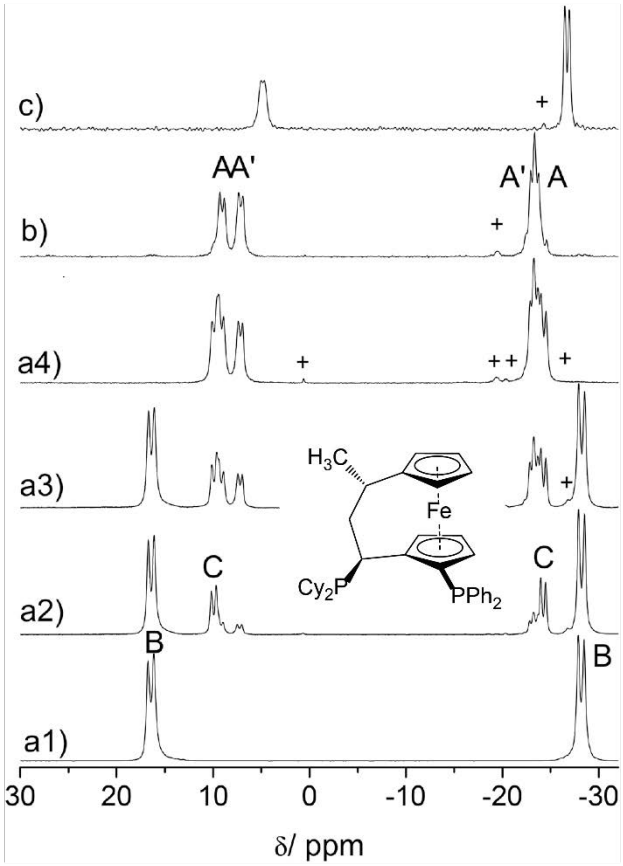

Figure 10: a1–a4: $^{31}P,^{1}H$ CP-MAS NMR spectra of a series of samples of a racemic *P,P*-[3]ferrocenophane (for a chemical structure of the *S*,*S*,S_{pl} enantiomer see the Figure) measured at 9.4 T with a spinning frequency of 10.0 kHz. (a1) Solvent (dichloromethane) removed by vacuum, (a2) crystallized overnight, (a3) crystallized over two days, (a4) crystallized over five days. The observed polymorphs are denoted with A, B and C. (b) $^{31}P,^{1}H$ CP-MAS-NMR spectrum obtained after exposing a sample of polymorph B to CH_2Cl_2 vapor at room temperature in a desiccator for 48 h. (c) $^{31}P,^{1}H$ CP-MAS-NMR spectrum of the optically pure compound (*S*,*S*,S_{pl}). + marks impurities. Reproduced with permission from reference [81].

We envision that solid-state NMR might develop into an important tool to detect the fate of solvent molecules in LAG-based organic reactions allowing addressing further mechanistic details of such processes.

Opportunity 5: Potential of MAS in *in-situ* approaches

As already mentioned in Section 2.2, *in-situ* MAS NMR studies of mechanochemical reactions might become feasible making use of the centrifugal pressures caused by MAS. Since MAS implies that the sample rotates around a fixed direction, a centrifugal force acts on the powder inside the MAS rotor. The centrifugal force dF_c acting on a material of mass *dm* inside a cylindrical rotor upon MAS can be estimated as

$$dF_c = dm \cdot r \cdot {\omega_r}^2 \quad (1)$$

where r represents the distance between the mass and the centre of the rotor and ω_r is the angular MAS frequency. If ρ is the density of the material, $dm = \rho dV$, where $dV = rdrd\theta dz$ is the element of the volume for a cylinder. The spinning-induced centrifugal force can, then, be calculated by

$$F_c = \int_0^{R_i} \int_0^{2\pi} \int_0^{l} {\omega_r}^2 r^2 dr d\theta dz = 2\pi l {\omega_r}^2 \frac{{R_i}^3}{3} \quad (2)$$

where l and R_i are the inner height and radius of the rotor, respectively. It is worth noting that the limits employed on the integrations imply that an entirely filled rotor is considered. Therefore, the spinning-induced centrifugal pressure, σ_c, acting on the inner rotor walls upon MAS can be estimated by:

$$\sigma_c = \frac{F_c}{A} = \frac{\rho \cdot \omega_r^2}{3} R_i^2 \quad (3)$$

where $A = 2\pi l R_i$ is the inner surface of the rotor wall. With this equation, the centrifugal pressure can be easily estimated for the different MAS rotor sizes employed in solid-state NMR. Figure 11 shows the centrifugal pressure in the inner rotor wall as a function of the applied MAS frequency. For this example, a samples density of 1758 kg/m^3 was assumed. Again, equation (3) was obtained by assuming that the MAS rotor is fully packed, i.e., all the inner volume of the rotor is filled with the material during spinning. Note, that such centrifugal pressures are much less than those occurring in ball-milling devices.

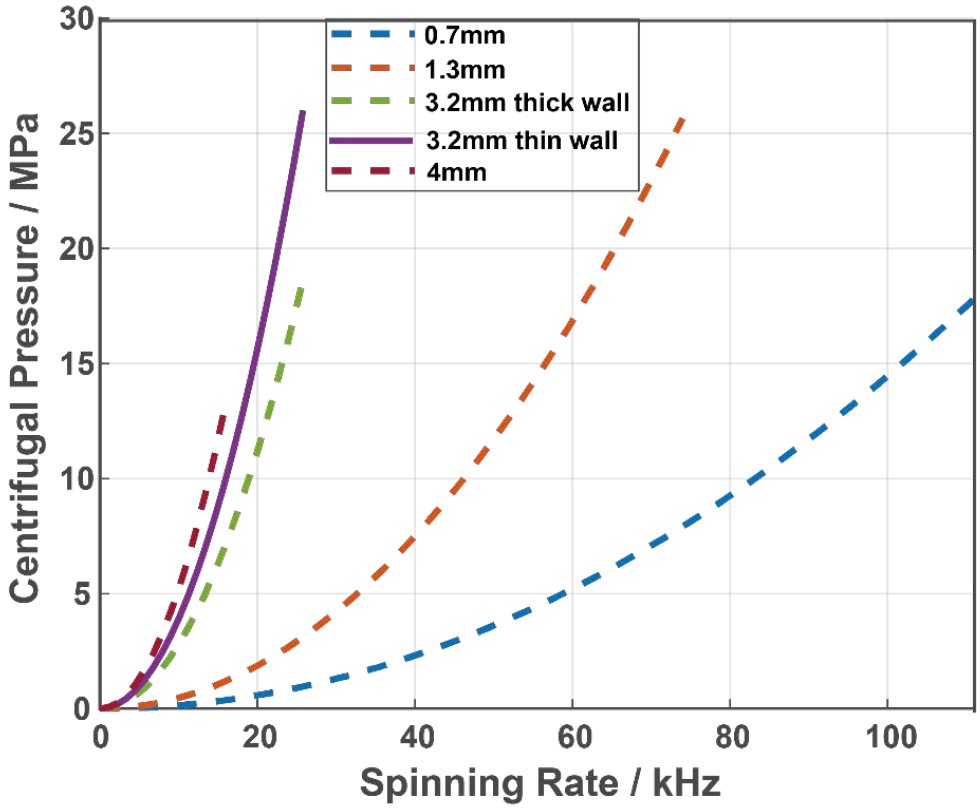

Figure 11: Centrifugal pressures at the inner rotor wall of an MAS rotor estimated (using equation (3)) for different MAS rotor sizes commonly employed in solid-state NMR. Adapted from reference [49] under CC BY-NC-ND 4.0 license (https://creativecommons.org/licenses/by-nc-nd/4.0/).

For some cases, it has been indeed possible to use MAS NMR as an *in-situ* spectroscopic technique. One example describes the halogen-bond formation between *p*-$C_6F_4I_2$ and Ph_3PO followed by ^{31}P MAS NMR.[82] Here the authors studied the influence of different effects, such as temperature, MAS frequency, and the presence of a liquid (acetonitrile) on the co-crystallization process. JMAYK (Johnson-Mehl-Avrami-Yerofeev-Kolmogorov) analysis of the normalized peak integrals revealed that the studied halogen-bond formation is predominantly dictated by a diffusion-controlled mechanism. In this study, the reagents were vortexed prior to the NMR experiments, which points to the fact that efficient mixing is required to initiate the halogen-bond formation.

Another example was the application of ^{13}C,^{1}H CP-MAS to monitor *in situ* the spontaneous co-crystallization of caffeine and malonic acid.[83] Here, the kinetics of the spontaneous co-crystallization was followed by recording ^{13}C,^{1}H CP-MAS spectra in intervals of 1 h for ^{13}C natural-abundant malonic acid and 80 seconds for (2-^{13}C)-isotope labeled malonic acid. For the latter, the authors followed the time-dependence of the NMR CH_2 resonances from

both, co-crystal and educts, and found no evidence for an intermediate phase in the studied co-crystallization process.

As detailed under *Opportunity 1*, we recently studied the bromination of a cyclic sulfoximine with *N*-bromosuccinimide (NBS).[49] With the intention to extend the *ex-situ* study to an *in-situ* MAS NMR approach, the two reagents were first mixed with a spatula and then filled into the NMR rotor. ^{13}C,^{1}H CP-MAS NMR spectra (see Figure 12) were taken successively between 0 to 100 hours. We were able to detect product formation, albeit in only ca. 20%, suggesting the critical importance of an efficient mixing process (as shown by solely mixing the educts on a magnetic-stirring device) in this organic mechanochemical transformation.

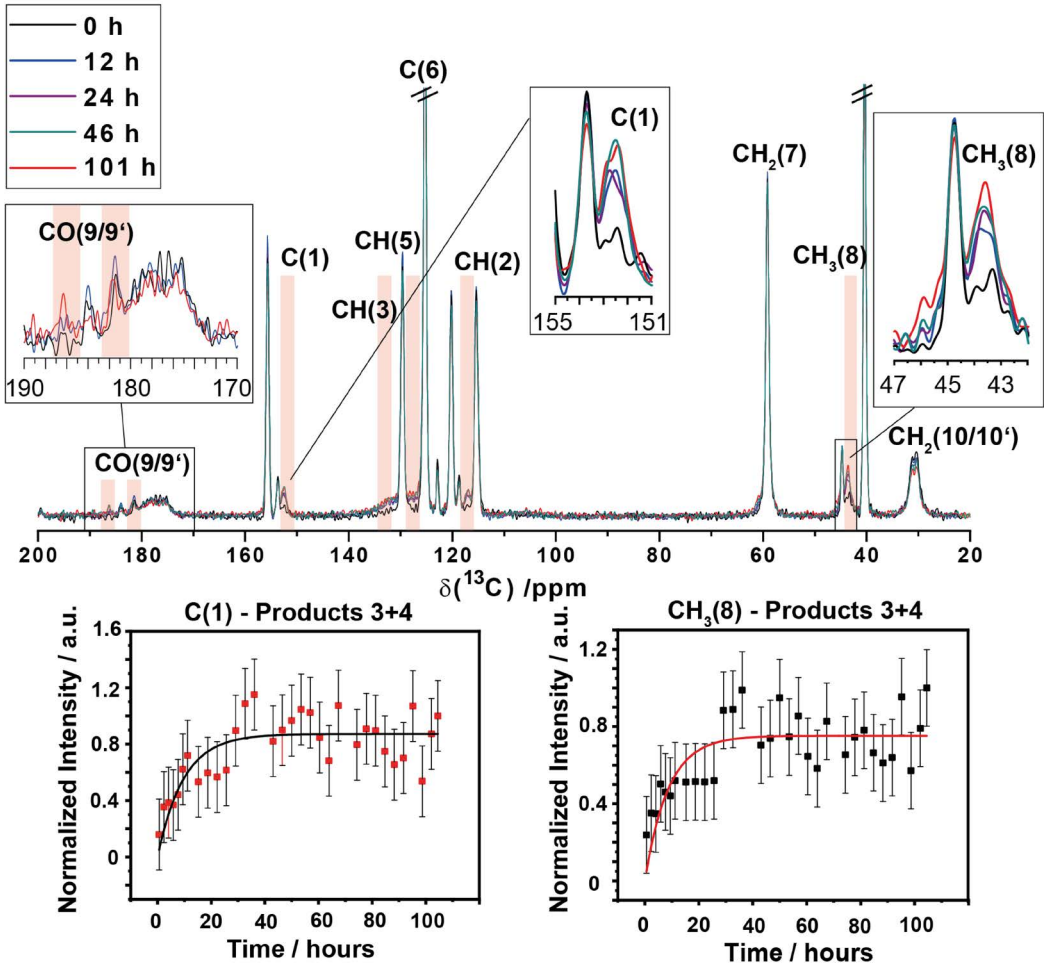

Figure 12: (top) ^{13}C, ^{1}H CP-MAS NMR spectra of the bromination reaction followed *in-situ* between 0 to 100 hours. Insets and red-coloured rectangles show peak positions where resonances from the products occur. (bottom) Normalized intensity of the NMR resonances vs. time for two representative product resonances. Solid lines represent a first-order kinetics fit. Adapted from reference [49] under CC BY-NC-ND 4.0 license (https://creativecommons.org/licenses/by-nc-nd/4.0/).

These first examples show that solid-state MAS NMR *in-situ* approaches to organic mechanochemistry are possible, although one must consider that mixing effects are only present (efficient) at the beginning of the MAS experiment, when the powder still redistributes within the rotor. Another factor playing an important role is that the pressure range available with MAS (see Figure 11) is limited by the geometry of the rotor and the maximum spinning frequency accessible. This however also opens an interesting opportunity. While in a ball mill the reaction outcome will rely on both, mixing and pressure effects (note that also temperature effects are discussed), solid-state NMR can disentangle these two factors by probing only the effect of pressure induced by MAS in a given organic mechanochemical process.

Opportunity 6: Protons as sensitive reporters for molecular-recognition events

As mentioned previously, solid-state NMR experiments under fast MAS conditions provide the opportunity for the acquisition of highly resolved proton spectra. On top of their ubiquitous presence and high sensitivity, these nuclei are of particular interest due to their engagement in noncovalent interactions, which are the cornerstone of molecular-recognition events in Chemistry and Biology. A particular advantage provided by solid-state NMR under fast MAS conditions relies on the fact that protons remain elusive to standard structure-determination techniques such as X-ray crystallography, due to low X-ray scattering factors of the hydrogen atom. As an example of the sensitivity of protons to noncovalent interactions, deshielded ^{1}H resonances can be used as an indication for the potential participation of the proton in a hydrogen bond. The effect of hydrogen-bonding on the ^{1}H NMR chemical shifts has been reported early on both in proteins and organic molecules, where protons have been demonstrated to be sensitive probes for the investigation of hydrogen-bonded systems.[84]

In the context of organic mechanochemistry, attractive applications are found in studying pharmaceutical co-crystals in which typically an active pharmaceutical ingredient (API) and one or more small organic molecules form a dimer by a dense network of hydrogen bonds. These systems have been widely investigated as an alternative approach in the context of site-selective delivery of active ingredients.[85] Many of such co-crystalline phases can be prepared under solvent-free conditions following green chemistry principles with mechanochemical synthesis,[9a, 86] and the kinetics of co-crystal formation can be further accelerated upon addition of small amounts of solvents during the grinding process (denoted as liquid assisted grinding, LAG).[87] Proton-detected solid-state NMR opens appealing analytical and physicochemical avenues to their characterization (see Figure 13 for a schematic

representation of co-crystal formation and its influence on ^{1}H solid-state NMR spectra).[88] As already mentioned, particularly attractive are the sub-milligram amount of powdered sample required, its atomic resolution, and the sensitivity to noncovalent interactions. Furthermore, proton-detected experiments do not rely on polarization transfer steps from other nuclei, such as the CP-technique discussed above. This enables ^{1}H-detected solid-state NMR experiments to be inherently quantitative, since the area of the peaks is directly proportional to the number of spins in the NMR rotor, for instance opening avenues for quantification of reaction conversion without requiring calibration steps.

Examples of the application of solid-state NMR approaches on several co-crystals and complexes have been early reported, where general state-of-the-art ^{1}H-detected solid-state NMR methods for a structural characterization are described[88-89]. Here, as soon as deshielded hydrogen-bonded protons are detected, a typical solid-state NMR toolbox for co-crystal investigation (*e.g.* employing NMR crystallography, see above) includes both ^{1}H-^{1}H homonuclear based experiments, such as Double-Quantum (DQ) MAS NMR[90], as well as ^{1}H-including heteronuclear approaches, in which at moderate MAS frequencies (<60 kHz) the X-nucleus is detected. As an example, informative experiments include ^{1}H-^{13}C HETCOR[91] for the determination of hydrogen donors and acceptors and the characterization of molecular association[88, 92] and ^{1}H-^{14}N HMQC[93] to detect intermolecular -N···H- hydrogen bonds.[92] Further ^{1}H-^{1}H dipolar connectivities can be probed among others using the Back-to-Back (BaBa) pulse sequence[94], where proximities can be observed from the homonuclear recoupling of ^{1}H-^{1}H dipolar couplings. This experiment can be applied not only to detect hydrogen bonding[95], but also aromatic π-π interactions.[96] With the advent of fast MAS, also proton-detected heteronuclear correlation experiments have been reported.[97]

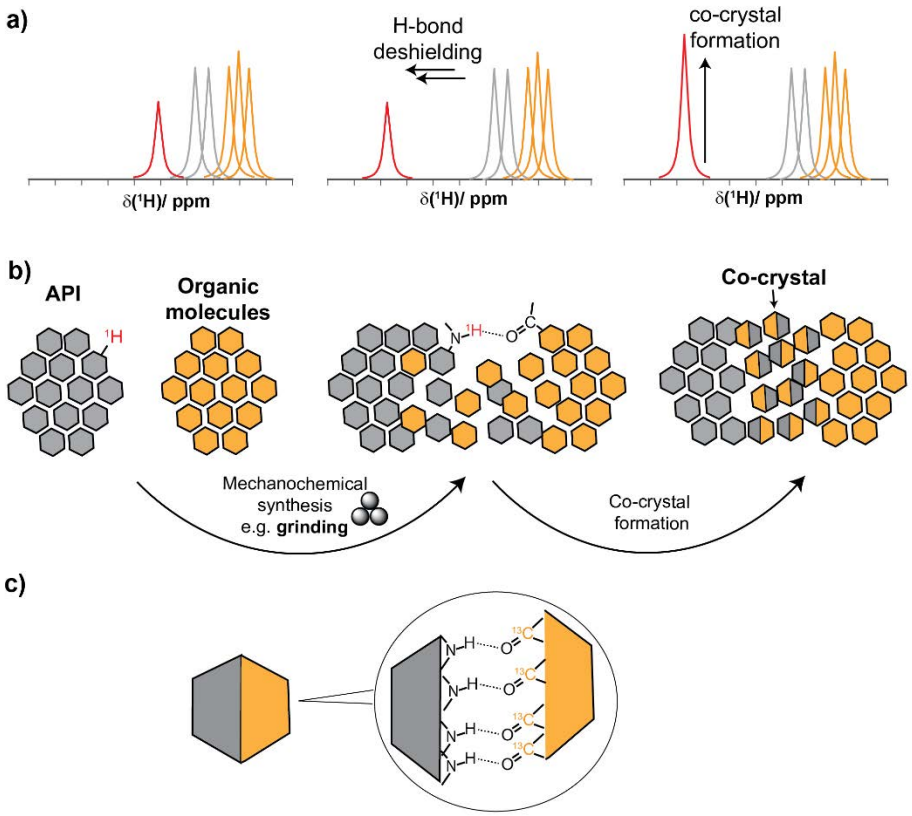

Figure 13: Schematic representation of co-crystal formation and its effects on ^{1}H MAS NMR spectra. **a** Observation of ^{1}H deshielding and co-crystal formation in a hypothetical ^{1}H MAS NMR spectrum. **b** Schematic representation of co-crystal formation upon mechanochemical energy input. **c** Schematic representation of hydrogen-bond formation responsible in co-crystal formation.

Opportunity 7: Isotope labelling for studying the incorporation of guest molecules in crystal lattices

Isotope labelling of organic molecules, for instance with ^{13}C and ^{15}N, significantly enhances the solid-state NMR signal and could be of high interest to unravel solid-state diffusion processes, where two solid phases merge, such as for instance in a "solid solution". In this context, Emmerling and co-workers described a very elegant example of employing ^{15}N isotope labelling in their report on the formation of a metastable phase of benzamide obtained by mechanochemical seeding with nicotinamide crystals.[98] The ^{15}N solid-state NMR spectra revealed that nicotinamide molecules were embedded in the benzamide crystal lattice, as concluded from different ^{15}N chemical-shift values compared to isolated nicotinamide. This example also clearly showed the limits of powder XRD, since no additional reflexes of nicotinamide pointing to its presence were observed in the solid samples. NMR, in contrast, even allows the detection of very small amounts of guest molecules embedded in crystal lattices.

In addition, a high potential is expected from ^{17}O isotope labelling, which also can be achieved in the ball mill.[99] ^{17}O offers among others the potential of being a quadrupolar

nucleus (I=5/2) enabling to access local structural information from the quadrupolar coupling parameters or even dynamic information.[100] For instance, the carbonyl groups of carboxylic acids can be labelled with ^{17}O. The labelling scheme is based on activating the carboxylic group by adding 1,1'-carbonyl-diimidazole and subsequent hydrolysis by ^{17}O labelled H_2O (both steps performed upon ball milling).[99] Various applications of this technique in the field of inorganic materials have been reported.[39]

3. Summary and future of solid-state NMR spectroscopy in organic mechanochemistry

As discussed in the seven opportunities listed above, we are convinced that solid-state NMR will further develop into an important tool to narrow the current gaps in today's missing mechanistic understanding of organic mechanochemical transformations. The most important advantages of solid-state NMR are the high sensitivity of the NMR observables for the local surrounding of nuclei (allowing, for instance, the distinction of polymorphs, pseudo-polymorphs or optical-pure/racemic associates), the quantitative nature, the dependence of NMR relaxation times on particle sizes, and the absent need to further process the sample for structural analysis (*e.g.*, dissolution as required for solution-state NMR).

While a successful *in-situ* study has been demonstrated by integrating a ball-milling device in a static solid-state NMR probe, such experiments under MAS conditions would in fact be highly desirable to achieve the required spectral resolution for applications in organic mechanosynthesis. However, such a setup remains rather unrealistic, since imbalances in the NMR rotor, for instance caused by ZrO_2 balls filled in the NMR rotor, strongly interfere with the MAS process. We are, however, currently exploring the use of very small ZrO_2 balls (diameters of 0.1 mm) for *in-situ* studies under MAS conditions. In addition, *in-situ* LAG could be investigated by *in-situ* solid-state NMR, with the possibility to even detect the fate of the liquid in the NMR spectra, *e.g.,* by using isotopic labelled solvents. A detailed quantification of the pressure distribution within the NMR rotor during MAS is urgently required, which for instance could be addressed by exploring the properties of mechanoluminescent materials,[101] whose emitted light could be used to quantify the centrifugal pressures experimentally or to initiate even photochemical reactions inside the NMR rotor.

The current strength of solid-state NMR is without doubts the *ex-situ* characterization of reaction products taken from ball-milling devices without any post-processing and a variety of successful examples have been reported. Particularly, proton-detected MAS experiments at fast MAS will enable to unravel solid-state molecular-recognition events by detecting

noncovalent interactions driving this process. This will open the way for NMR-crystallographic approaches, as well as to probe recognition events by long-range correlation experiments exploring spin diffusion.

Of particular interest is to derive a thorough mechanistic understanding of the solid-state molecular-recognition processes. How do the molecules, *e.g.*, the substrates of an organic reaction, recognize each other in the solid state? How does the solid-state diffusion process work? What is the influence of the pressure on the reaction and how can we disentangle this from the mixing event? Possibly, answers will be obtained from solid-state NMR, for instance also by benefitting from isotope-labelling approaches in which the fate of an isotope labelled starting material during a reaction can be followed over the course of the reaction, particularly of interest in cases where solid-state diffusion drives solid-solid reactions. Here, it might even be of advantage that the centrifugal pressure induced by MAS is lower than the pressure expected in ball-milling devices and that the reaction kinetics are slowed down to such an extent that *in-situ* solid-state NMR studies become possible.[49]

However, pressure and mixing are not the only sources of energy input in mechanochemical transformations. Also, applications of sonication, for instance in the field of polymer sciences, have been reported.[102] While again interference with MAS might complicate *in-situ* studies, the NMR rotor could be ejected from the NMR probe and directed in an ultrasound device and subsequently inserted in the probe again. Inspiration for such setups could for instance be obtained from dynamic nuclear polarization (DNP) setups.

However, it is rather obvious that solid-state NMR needs to be part of the entire toolbox of structure-determination approaches applied so far, especially considering advanced quantum-chemical approaches (for a summary of key advantages and disadvantages for several players explored in experimentally characterizing reaction products in organic mechanochemistry see Figure 14). Altogether, with this overview, we intended to share our view on solid-state NMR studies in the highly emerging field of mechanochemistry.

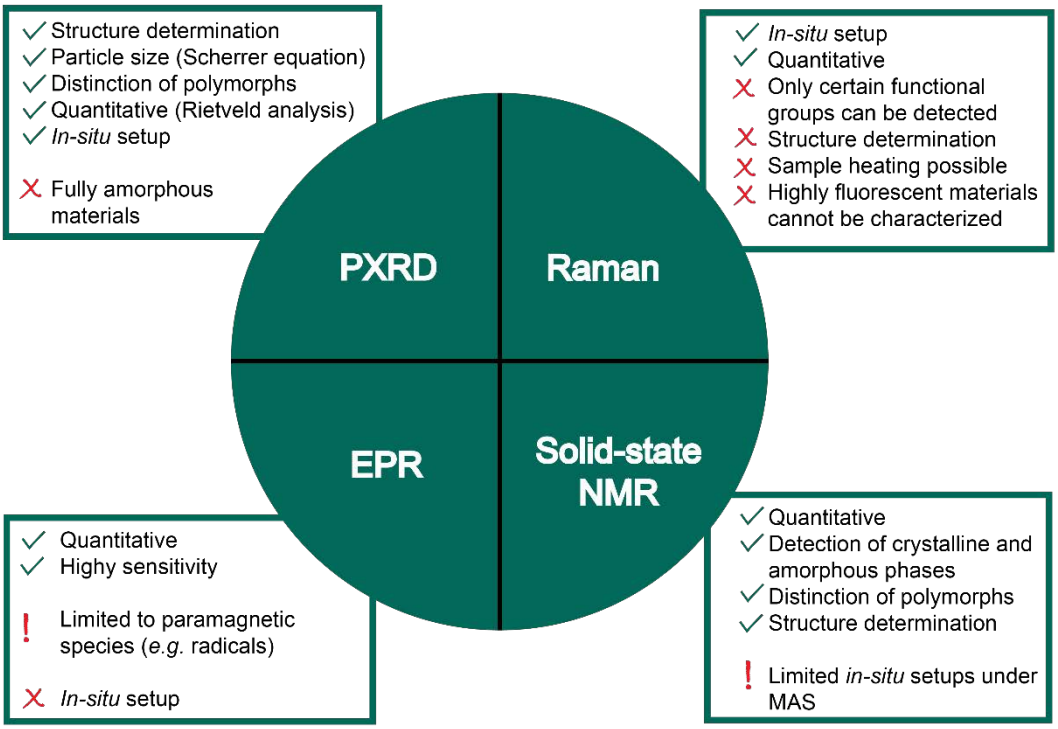

Figure 14: Schematic overview of selected pros and cons of powder XRD, RAMAN, EPR and solid-state NMR techniques employed in organic mechanochemistry.

Acknowledgements

All authors appreciate the funding by the Deutsche Forschungsgemeinschaft (DFG, German Research Foundation) under Germany's Excellence Strategy – Exzellenzcluster 2186 "The Fuel Science Center". T.W. acknowledges support from the Deutsche Forschungsgemeinschaft (DFG, German Research Foundation, project number 455240421 and Heisenberg fellowship, project number 455238107) and the Max Planck Society. We acknowledge helpful discussions with Dr. Francesco Puccetti and Calogero Quaranta (both RWTH Aachen University) and thank Dr. Baran Uluca-Yazgi and Dr. Rıza Dervişoğlu (both MPI CEC) for providing the Figure of the NMR rotors.

References

[1] a) L. Takacs, *JOM* **2000**, *52*, 12-13; b) L. Takacs, *Chem. Soc. Rev.* **2013**, *42*, 7649-7659.

[2] a) S. L. James, C. J. Adams, C. Bolm, D. Braga, P. Collier, T. Friščić, F. Grepioni, K. D. M. Harris, G. Hyett, W. Jones, A. Krebs, J. Mack, L. Maini, A. G. Orpen, I. P. Parkin, W. C. Shearouse, J. W. Steed, D. C. Waddell, *Chem. Soc. Rev.* **2012**, *41*, 413-447; b) A. A. L. Michalchuk, E. V. Boldyreva, A. M. Belenguer, F. Emmerling, V. V. Boldyrev, *Front. Chem.* **2021**, *9*, 685789; c) F. Cuccu, L. De Luca, F. Delogu, E. Colacino, N. Solin, R. Mocci, A. Porcheddu, *ChemSusChem* **2022**, *15*, e202200362.

[3] K. S. Suslick, *Faraday Discuss.* **2014**, *170*, 411-422.

[4] E. Boldyreva, *Chem. Soc. Rev.* **2013**, *42*, 7719-7738.

[5] For reviews, see: a) J. L. Do, T. Friščić, *ACS Cent. Sci.* **2017**, *3*, 13-19; b) J. G. Hernández, C. Bolm, *J. Org. Chem.* **2017**, *82*, 4007-4019; c) J. Andersen, J. Mack, *Green Chem.* **2018**, *20*, 1435-1443; d) V. Štrukil, *Synlett* **2018**, *29*, 1281-1288; e) M. Leonardi, M. Villacampa, J. C. Menéndez, *Chem. Sci.* **2018**, *9*, 2042-2064; f) C. Bolm, J. G. Hernández, *ChemSusChem* **2018**, *11*, 1410-1420; g) D. Tan, T. Friščić, *Eur. J. Org. Chem.* **2018**, *2018*, 18-33; h) J. L. Howard, Q. Cao, D. L. Browne, *Chem. Sci.* **2018**, *9*, 3080-3094; i) E. Colacino, A. Porcheddu, C. Charnay, F. Delogu, *Reaction Chem. Eng.* **2019**, *4*, 1179-1188; j) A. Porcheddu, E. Colacino, L. De Luca, F. Delogu, *ACS Catal.* **2020**, *10*, 8344-8394; k) K. Kubota, H. Ito, *Trends Chem.* **2020**, *2*, 1066-1081; l) T. Friščić, C. Mottillo, H. M. Titi, *Angew. Chem. Int. Ed.* **2020**, *59*, 1018-1029; *Angew. Chem.* **2020**, *132*, 1030-1041; m) M. Pérez-Venegas, E. Juaristi, *ACS Sustainable Chem. Eng.* **2020**, *8*, 8881-8893; n) W. Pickhardt, S. Grätz, L. Borchardt, *Chem. Eur. J.* **2020**, *26*, 12903-12911; o) I. N. Egorov, S. Santra, D. S. Kopchuk, I. S. Kovalev, G. V. Zyryanov, A. Majee, B. C. Ranu, V. L. Rusinov, O. N. Chupakhin, *Green Chem.* **2020**, *22*, 302-315; p) D. Virieux, F. Delogu, A. Porcheddu, F. García, E. Colacino, *J. Org. Chem.* **2021**, *86*, 13885-13894; q) O. V. Lapshin, E. V. Boldyreva, V. V. Boldyrev, *Russ. J. Inorg. Chem.* **2021**, *66*, 433-453; r) M. T. J. Williams, L. C. Morrill, D. L. Browne, *ChemSusChem* **2022**, *15*, e202102157; s) M. J. Xuan, C. Schumacher, C. Bolm, R. Göstl, A. Herrmann, *Adv. Sci.* **2022**, *9*, 2105497; t) V. Martinez, T. Stolar, B. Karadeniz, I. Brekalo, K. Užarević, *Nat. Rev. Chem.* **2023**, *7*, 51-65.

[6] a) K. J. Ardila-Fierro, J. G. Hernández, *ChemSusChem* **2021**, *14*, 2145-2162; b) P. Sharma, C. Vetter, E. Ponnusamy, E. Colacino, *ACS Sustainable Chem. Eng.* **2022**, *10*, 5110-5116.

[7] For selected work, see: a) O. Galant, G. Cerfeda, A. S. McCalmont, S. L. James, A. Porcheddu, F. Delogu, D. E. Crawford, E. Colacino, S. Spatari, *ACS Sustainable Chem. Eng.* **2022**, *10*, 1430-1439; b) R. R. A. Bolt, J. A. Leitch, A. C. Jones, W. I. Nicholson, D. L. Browne, *Chem. Soc. Rev.* **2022**, *51*, 4243-4260; c) E. C. Gaudino, G. Grillo, M. Manzoli, S. Tabasso, S. Maccagnan, G. Cravotto, *Molecules* **2022**, *27*, 449; d) A. A. L. Michalchuk, K. S. Hope, S. R. Kennedy, M. V. Blanco, E. V. Boldyreva, C. R. Pulham, *Chem. Commun.* **2018**, *54*, 4033-4036; e) L. Gonnet, C. B. Lennox, J. L. Do, I. Malvestiti, S. G. Koenig, K. Nagapudi, T. Friščić, *Angew. Chem. Int. Ed.* **2022**, *61*, e202115030; *Angew. Chem.* **2022**, *134*, e202115030.

[8] a) J. Stroh, N. Z. Ali, C. Maierhofer, F. Emmerling, *ACS Omega* **2019**, *4*, 7734-7737; b) E. Colacino, V. Isoni, D. Crawford, F. García, *Trends Chem.* **2021**, *3*, 335-339.

[9] a) T. Friščić, *Chem. Soc. Rev.* **2012**, *41*, 3493-3510; b) A. Bose, P. Mal, *Beilstein J. Org. Chem.* **2019**, *15*, 881-900; c) T. Stolar, K. Užarević, *CrystEngComm* **2020**, *22*, 4511-4525.

[10] a) A. Delori, T. Friščić, W. Jones, *CrystEngComm* **2012**, *14*, 2350-2362; b) D. Hasa, W. Jones, *Adv. Drug Del. Rev.* **2017**, *117*, 147-161; c) M. Solares-Briones, G. Coyote-Dotor, J. C. Páez-Franco, M. R. Zermeño-Ortega, C. M. D. Contreras, D. Canseco-González, A. Avila-Sorrosa, D. Morales-Morales, J. M. Germán-Acacio, *Pharmaceutics* **2021**, *13*, 790.

[11] C. Weidenthaler, *Crystals* **2022**, *12*, 345.

[12] Fon an example, see: K. J. Ardila-Fierro, S. Lukin, M. Etter, K. Užarević, I. Halasz, C. Bolm, J. G. Hernández, *Angew. Chem. Int. Ed.* **2020**, *59*, 13458-13462; *Angew. Chem.* **2020**, *132*, 13560-13564.

[13] H. Kohlmann, *Eur. J. Inorg. Chem.* **2019**, 4174-4180.

[14] T. Stauch, A. Dreuw, *Chem. Rev.* **2016**, *116*, 14137-14180.

[15] C. F. Holder, R. E. Schaak, *ACS Nano* **2019**, *13*, 7359-7365.

[16] For a recent study where this analysis was essential, see: F. Puccetti, T. Rinesch, S. Suljić, K. Rahimi, A. Herrmann, C. Bolm, *Chem* **2023**, *9*, 1-15.

[17] a) F. Fischer, A. Heidrich, S. Greiser, S. Benemann, K. Rademann, F. Emmerling, *Cryst. Growth Des.* **2016**, *16*, 1701-1707; b) D. Hasa, E. Miniussi, W. Jones, *Cryst.*

Growth Des. **2016**, *16*, 4582-4588; c) H. Kulla, C. Becker, A. A. L. Michalchuk, K. Linberg, B. Paulus, F. Emmerling, *Cryst. Growth Des.* **2019**, *19*, 7271-7279.

[18] a) T. Friščić, I. Halasz, P. J. Beldon, A. M. Belenguer, F. Adams, S. A. J. Kimber, V. Honkimäki, R. E. Dinnebier, *Nat. Chem.* **2013**, *5*, 66-73; b) I. Halasz, S. A. J. Kimber, P. J. Beldon, A. M. Belenguer, F. Adams, V. Honkimäki, R. C. Nightingale, R. E. Dinnebier, T. Friščić, *Nat. Prot.* **2013**, *8*, 1718-1729; c) I. Halasz, A. Puškarić, S. A. J. Kimber, P. J. Beldon, A. M. Belenguer, F. Adams, V. Honkimäki, R. E. Dinnebier, B. Patel, W. Jones, V. Štrukil, T. Friščić, *Angew. Chem. Int. Ed.* **2013**, *52*, 11538-11541; *Angew. Chem,* **2013**, *125*, 11752-11755; d) I. Halasz, T. Friščić, S. A. J. Kimber, K. Užarević, A. Puškarić, C. Mottillo, P. Julien, V. Štrukil, V. Honkimäki, R. E. Dinnebier, *Faraday Discuss.* **2014**, *170*, 203-221; e) V. Ban, Y. Sadikin, M. Lange, N. Tumanov, Y. Filinchuk, R. Cerny, N. Casati, *Anal. Chem.* **2017**, *89*, 13176-13181.

[19] a) G. I. Lampronti, A. A. L. Michalchuk, P. P. Mazzeo, A. M. Belenguer, J. K. M. Sanders, A. Bacchi, F. Emmerling, *Nat. Commun.* **2021**, *12*, 6134; b) A. A. L. Michalchuk, F. Emmerling, *Angew. Chem. Int. Ed. Engl.* **2022**, *61*, e202117270; *Angew. Chem.* **2022**, *134*, e202117270.

[20] S. Lukin, K. Užarević, I. Halasz, *Nat. Prot.* **2021**, *16*, 3492-3521.

[21] X. H. Ma, W. B. Yuan, S. E. J. Bell, S. L. James, *Chem. Commun.* **2014**, *50*, 1585-1587.

[22] a) D. Gracin, V. Štrukil, T. Friščić, I. Halasz, K. Užarević, *Angew. Chem. Int. Ed.* **2014**, *53*, 6193-6197; *Angew. Chem.* **2014**, *126*, 6307-6311; b) I. Sović, S. Lukin, E. Meštrović, I. Halasz, A. Porcheddu, F. Delogu, P. C. Ricci, F. Caron, T. Perilli, A. Dogan, E. Colacino, *ACS Omega* **2020**, *5*, 28663-28672; c) F. Puccetti, S. Lukin, K. Užarević, E. Colacino, I. Halasz, C. Bolm, J. G. Hernández, *Chem. Eur. J.* **2022**, *28*, e202104409.

[23] a) L. Batzdorf, F. Fischer, M. Wilke, K. J. Wenzel, F. Emmerling, *Angew. Chem. Int. Ed.* **2015**, *54*, 1799-1802; *Angew. Chem.* **2015**, *127*, 1819-1822; b) Z. Sun, B. Lin, X. Yang, B. Zhao, H. Zhang, Q. Dong, L. Zhong, S. Zhang, M. Zhang, X. Xu, *Curr. Top. Med. Chem.* **2022**, *23*.

[24] D. V. Aleksanyan, S. G. Churusova, V. V. Brunova, A. S. Peregudov, A. M. Shakhov, E. Y. Rybalkina, Z. S. Klemenkova, E. G. Kononova, G. L. Denisov, V. A. Kozlov, *Dalton Trans.* **2021**, *50*, 16726-16738.

[25] J. S. González-González, R. Jiménez-López, D. Ortegòn-Reyna, G. Gonzalez-Carrillo, F. J. Martínez-Martínez, *Appl. Sci.* **2021**, *11*, 3810.

[26] S. Andini, A. Bolognese, D. Formisano, M. Manfra, F. Montagnaro, L. Santoro, *Chemosphere* **2012**, *88*, 548-553.

[27] R. P. Kaiser, E. F. Krake, L. Backer, J. Urlaub, W. Baumann, N. Handler, H. Buschmann, T. Beweries, U. Holzgrabe, C. Bolm, *Chem. Commun.* **2021**, *57*, 11956-11959.

[28] R. L. Frost, É. Makó, J. Kristóf, J. T. Kloprogge, *Spectrochim. Acta A* **2002**, *58*, 2849-2859.

[29] C. Bolm, J. G. Hernández, *Angew. Chem. Int. Ed.* **2019**, *58*, 3285-3299; *Angew. Chem.* **2019**, *131*, 3320-3335.

[30] T. Rathmann, H. Petersen, S. Reichle, W. Schmidt, A. P. Amrute, M. Etter, C. Weidenthaler, *Rev. Sci. Instrum.* **2021**, *92*, 114102.

[31] M. M. Roessler, E. Salvadori, *Chem. Soc. Rev.* **2018**, *47*, 2534-2553.

[32] a) K. Ravindranadh, B. Babu, C. V. Reddy, J. Shim, M. C. Rao, R. V. S. S. N. Ravikumar, *Appl. Magn. Reson.* **2015**, *46*, 1-15; b) A. I. Kokorin, A. N. Streletskii, I. V. Kolbanev, A. B. Borunova, Y. N. Degtyarev, A. V. Leonov, D. G. Permenov, E. A. Konstantinova, *J. Phys. Chem. C* **2019**, *123*, 19991-19998.

[33] K. Gobindlal, Z. Zujovic, P. Yadav, J. Sperry, C. C. Weber, *J. Phys. Chem. C* **2021**, *125*, 20877-20886.

[34] M. Kuzuya, S. Kondo, K. Murase, *J. Phys. Chem.* **1993**, *97*, 7800-7802.

[35] V. P. Balema, I. Z. Hlova, S. L. Carnahan, M. Seyedi, O. Dolotko, A. J. Rossini, I. Luzinov, *New J. Chem.* **2021**, *45*, 4867-4867.

[36] K. Imato, A. Irie, T. Kosuge, T. Ohishi, M. Nishihara, A. Takahara, H. Otsuka, *Angew. Chem. Int. Ed.* **2015**, *54*, 6168-6172; *Angew. Chem.* **2015**, *127*, 6266-6270.

[37] A. V. Dushkin, I. B. Troitskaya, V. V. Boldyrev, I. A. Grigor'ev, *Russ. Chem. Bull.* **2005**, *54*, 1155-1159.

[38] P. van Bonn, C. Bolm, J. G. Hernández, *Chem. Eur. J.* **2020**, *26*, 2576-2580.

[39] For an analogous analysis of the potential of solid-state NMR in the chemistry of inorganic components of materials, see: C. Leroy, T.-X. Métro, D. Laurencin, in *Comp. Inorg. Chem. III* **2023**, pp. 514-533.

[40] a) I. J. Lowe, *Phys. Rev. Lett.* **1959**, *2*, 285-287; b) E. R. Andrew, A. Bradbury, R. G. Eades, *Nature* **1958**, *182*, 1659-1659.

[41] a) A. Samoson, *J. Magn. Reson.* **2019**, *306*, 167-172; b) E. C. Y. Yuan, S. J. Huang, H. C. Huang, J. Sinkkonen, A. Oss, M. L. Org, A. Samoson, H. C. Tai, J. C. C. Chan, *Chem. Commun.* **2021**, *57*, 4110-4113; c) M. Schledorn, A. A. Malär, A. Torosyan, S.

Penzel, D. Klose, A. Oss, M. L. Org, S. S. Wang, L. Lecoq, R. Cadalbert, A. Samoson, A. Böckmann, B. H. Meier, *Chembiochem* **2020**, *21*, 2540-2548.

[42] P. Chen, B. J. Albert, C. Gao, N. Alaniva, L. E. Price, F. J. Scott, E. P. Saliba, E. L. Sesti, P. T. Judge, E. W. Fisher, A. B. Barnes, *Sci. Adv.* **2018**, *4*, eaau1540.

[43] a) A. Böckmann, M. Ernst, B. H. Meier, *J. Magn. Reson.* **2015**, *253*, 71-79; b) U. Sternberg, R. Witter, I. Kuprov, J. M. Lamley, A. Oss, J. R. Lewandowski, A. Samoson, *J. Magn. Reson.* **2018**, *291*, 32-39.

[44] a) I. Bertini, L. Emsley, M. Lelli, C. Luchinat, J. F. Mao, G. Pintacuda, *J. Am. Chem. Soc.* **2010**, *132*, 5558-5559; b) A. J. Pell, G. Pintacuda, C. P. Grey, *Prog. Nucl. Magn. Reson. Spectrosc.* **2019**, *111*, 1-271.

[45] T. Le Marchand, T. Schubeis, M. Bonaccorsi, P. Paluch, D. Lalli, A. J. Pell, L. B. Andreas, K. Jaudzems, J. Stanek, G. Pintacuda, *Chem. Rev.* **2022**, *122*, 9943-10018.

[46] a) T. Gullion, J. Schaefer, *J. Magn. Reson.* **1989**, *81*, 196-200; b) T. Gullion, *Conc. Magn. Reson.* **1998**, *10*, 277-289.

[47] J. G. Schiffmann, F. Emmerling, I. C. B. Martins, L. van Wüllen, *Solid State Nucl. Magn. Reson.* **2020**, *109*, 101687.

[48] C. M. Quinn, R. Zadorozhnyi, J. Struppe, I. V. Sergeyev, A. M. Gronenborn, T. Polenova, *Anal. Chem.* **2021**, *93*, 13029-13037.

[49] E. Bartalucci, C. Schumacher, L. Hendrickx, F. Puccetti, I. D. A. Silva, R. Dervişoğlu, R. Puttreddy, C. Bolm, T. Wiegand, *Chem. Eur. J.* **2023**, *e202203466*.

[50] S. Gupta, T. Kobayashi, I. Z. Hlova, J. F. Goldston, M. Pruski, V. K. Pecharsky, *Green Chem.* **2014**, *16*, 4378-4388.

[51] T. Kobayashi, O. Dolotko, S. Gupta, V. K. Pecharsky, M. Pruski, *J. Phys. Chem. C* **2018**, *122*, 1955-1962.

[52] V. P. Balema, J. W. Wiench, M. Pruski, V. K. Pecharsky, *Chem. Commun.* **2002**, 724-725.

[53] V. P. Balema, J. W. Wiench, M. Pruski, V. K. Pecharsky, *Chem. Commun.* **2002**, 1606-1607.

[54] A. Wroblewska, P. Paluch, E. Wielgus, G. Bujacz, M. K. Dudek, M. J. Potrzebowski, *Org. Lett.* **2017**, *19*, 5360-5363.

[55] a) V. A. Soloshonok, H. Ueki, M. Yasumoto, S. Mekala, J. S. Hirschi, D. A. Singleton, *J. Am. Chem. Soc.* **2007**, *129*, 12112-12113; b) M. Albrecht, V. A. Soloshonok, L. Schrader, M. Yasumoto, M. A. Suhm, *J. Fluorine Chem.* **2010**, *131*, 495-504.

[56] F. Puccetti, C. Quaranta, E. Bartalucci, I. D. A. Silva, T. Wiegand, C. Bolm, *to be published*.

[57] D. Crawford, A. Porcheddu, A. McCalmont, F. Delogu, S. James, E. Colacino, *ACS Sustainable Chem Eng* **2020**, *8*, 12230-12238.

[58] a) P. Hodgkinson, *Prog. Nucl. Magn. Reson. Spectrosc.* **2020**, *118-119*, 10-53; b) S. A. Southern, D. L. Bryce, *Annu. Rep. NMR Spectrosc.* **2021**, *102*, 1-80; c) C. Martineau, J. Senker, F. Taulelle, *Annu. Rep. NMR Spectrosc.* **2014**, *82*, 1-57.

[59] W. I. David, K. Shankland, L. B. McCusker, C. Baerlocher, *Structure determination from powder diffraction data, Vol. 13*, OUP Oxford, **2006**.

[60] a) C. J. Pickard, F. Mauri, *Phys. Rev. B* **2001**, *63*, 245101; b) C. Bonhomme, C. Gervais, F. Babonneau, C. Coelho, F. Pourpoint, T. Azais, S. E. Ashbrook, J. M. Griffin, J. R. Yates, F. Mauri, C. J. Pickard, *Chem. Rev.* **2012**, *112*, 5733-5779.

[61] S. E. Ashbrook, D. McKay, *Chem. Commun.* **2016**, *52*, 7186-7204.

[62] R. K. Harris, *Solid State Sci.* **2004**, *6*, 1025-1037.

[63] C. S. Vojvodin, S. T. Holmes, L. K. Watanabe, J. M. Rawson, R. W. Schurko, *CrystEngComm* **2022**, *24*, 2626-2641.

[64] A. A. Peach, D. A. Hirsh, S. T. Holmes, R. W. Schurko, *CrystEngComm* **2018**, *20*, 2780-2792.

[65] C. Leroy, T. X. Métro, I. V. Hung, Z. H. Gan, C. Gervais, D. Laurencin, *Chem. Mater.* **2022**.

[66] M. Descamps, J. F. Willart, *Adv. Drug Del. Rev.* **2016**, *100*, 51-66.

[67] R. Lefort, A. De Gusseme, J. F. Willart, F. Danede, M. Descamps, *Int. J. Pharm.* **2004**, *280*, 209-219.

[68] S. Ahlawat, K. R. Mote, N. A. Lakomek, V. Agarwal, *Chem. Rev.* **2022**, *122*, 9643-9737.

[69] R. Teeaar, E. Lippmaa, *Polym. Bull.* **1984**, *12*, 315-318.

[70] W. Papawassiliou, J. P. Carvalho, N. Panopoulos, Y. Al Wahedi, V. K. S. Wadi, X. Lu, K. Polychronopoulou, J. B. Lee, S. Lee, C. Y. Kim, H. J. Kim, M. Katsiotis, V. Tzitzios, M. Karagianni, M. Fardis, G. Papavassiliou, A. J. Pell, *Nat. Commun.* **2021**, *12*, 4334.

[71] K. E. Dempah, J. W. Lubach, E. J. Munson, *Mol. Pharm.* **2017**, *14*, 1319-1319.

[72] J. W. Lubach, D. W. Xu, B. E. Segmuller, E. J. Munson, *J. Pharm. Sci.* **2007**, *96*, 777-787.

[73] K. E. Dempah, D. H. Barich, A. M. Kaushal, Z. Zong, S. D. Desai, R. Suryanarayanan, L. Kirsch, E. J. Munson, *AAPS PharmSciTech* **2013**, *14*, 19-28.

[74] a) I. R. Speight, I. Huskic, M. Arhangelskis, H. M. Titi, R. S. Stein, T. P. Hanusa, T. Friščić, *Chem. Eur. J.* **2020**, *26*, 1811-1818; b) L. S. Germann, M. Arhangelskis, R. Stein, M. Etter, R. E. Dinnebier, T. Friščić, *ChemRxiv* **2020**, doi: 10.26434/chemrxiv.11829414.v11829411.

[75] a) D. Hasa, M. Marosa, D.-K. i. Bučar, M. K. Corpinot, D. Amin, B. Patel, W. Jones, *Cryst. Growth Des.* **2019**, *20*, 1119-1129; b) S. Lukin, T. Stolar, M. Tireli, M. V. Blanco, D. Babic, T. Friščić, K. Užarević, I. Halasz, *Chem. Eur. J.* **2017**, *23*, 13941-13949; c) S. M. Oburn, O. A. Ray, L. R. MacGillivray, *Cryst. Growth Des.* **2018**, *18*, 2495-2501.

[76] B. D. Altheimer, S. Pagola, M. Zeller, M. A. Mehta, *Cryst. Growth Des.* **2013**, *13*, 3447-3453.

[77] a) C. E. Hughes, K. D. M. Harris, *J. Phys. Chem. A* **2008**, *112*, 6808-6810; b) C. E. Hughes, K. D. M. Harris, *Chem. Commun.* **2010**, *46*, 4982-4984.

[78] S. J. Kitchin, S. B. Ahn, K. D. M. Harris, *J. Phys. Chem. A* **2002**, *106*, 7228-7234.

[79] C. Schumacher, D. E. Crawford, B. Raguz, R. Glaum, S. L. James, C. Bolm, J. G. Hernández, *Chem. Commun.* **2018**, *54*, 8355-8358.

[80] H. Kulla, S. Greiser, S. Benemann, K. Rademann, F. Emmerling, *Cryst. Growth Des.* **2017**, *17*, 1190-1196.

[81] T. Wiegand, D. Ludeker, G. Brunklaus, K. Bussmann, G. Kehr, G. Erker, H. Eckert, *Dalton Trans.* **2014**, *43*, 12639-12647.

[82] Y. J. Xu, L. Champion, B. Gabidullin, D. L. Bryce, *Chem. Commun.* **2017**, *53*, 9930-9933.

[83] V. S. Mandala, S. J. Loewus, M. A. Mehta, *J. Phys. Chem. Lett.* **2014**, *5*, 3340-3344.

[84] a) E. Brunner, U. Sternberg, *Prog. Nucl. Magn. Reson. Spectrosc.* **1998**, *32*, 21-57; b) R. K. Harris, P. Y. Ghi, R. B. Hammond, C. Y. Ma, K. J. Roberts, *Chem. Commun.* **2003**, 2834-2835; c) J. R. Yates, T. N. Pham, C. J. Pickard, F. Mauri, A. M. Amado, A. M. Gil, S. P. Brown, *J. Am. Chem. Soc.* **2005**, *127*, 10216-10220; d) J. Schmidt, A. Hoffmann, H. W. Spiess, D. Sebastiani, *J. Phys. Chem. B* **2006**, *110*, 23204-23210; e) A. S. Tatton, T. N. Pham, F. G. Vogt, D. Iuga, A. J. Edwards, S. P. Brown, *Mol. Pharm.* **2013**, *10*, 999-1007; f) G. Wagner, A. Pardi, K. Wuthrich, *J. Am. Chem. Soc.* **1983**, *105*, 5948-5949; g) A. A. Malär, L. A. Völker, R. Cadalbert, L. Lecoq, M. Ernst, A. Böckmann, B. H. Meier, T. Wiegand, *J. Phys. Chem. B* **2021**, *125*, 6222-6230.

[85] J. W. Steed, *Trends Pharmacol. Sci.* **2013**, *34*, 185-193.

[86] D. Braga, L. Maini, F. Grepioni, *Chem. Soc. Rev.* **2013**, *42*, 7638-7648.

[87] N. Shan, F. Toda, W. Jones, *Chem. Commun.* **2002**, 2372-2373.

[88] F. G. Vogt, J. S. Clawson, M. Strohmeier, A. J. Edwards, T. N. Pham, S. A. Watson, *Cryst. Growth Des.* **2009**, *9*, 921-937.

[89] D. H. Zhou, C. M. Rienstra, *Angew. Chem. Int. Ed.* **2008**, *47*, 7328-7331; *Angew. Chem.* **2008**, *120*, 7438-7441.

[90] a) S. P. Brown, *Prog. Nucl. Magn. Reson. Spectrosc.* **2007**, *50*, 199-251; b) S. P. Brown, *Solid State Nucl. Magn. Reson.* **2012**, *41*, 1-27.

[91] a) K. Saalwächter, R. Graf, H. W. Spiess, *J. Magn. Reson.* **1999**, *140*, 471-476; b) P. Caravatti, L. Braunschweiler, R. R. Ernst, *Chem. Phys. Lett.* **1983**, *100*, 305-310.

[92] Z. Rehman, W. T. Franks, B. Nguyen, H. F. Schmidt, G. Scrivens, S. P. Brown, *J. Pharm. Sci.* **2023**, doi: 10.1016/j.xphs.2023.1002.1022.

[93] a) A. S. Tatton, J. P. Bradley, D. Iuga, S. P. Brown, *Z. Phys. Chem.* **2012**, *226*, 1187-1204; b) S. Cavadini, *Prog. Nucl. Magn. Reson. Spectrosc.* **2010**, *56*, 46-77; c) S. Cavadini, S. Antonijevic, A. Lupulescu, G. Bodenhausen, *J. Magn. Reson.* **2006**, *182*, 168-172.

[94] a) K. Saalwächter, F. Lange, K. Matyjaszewski, C. F. Huang, R. Graf, *J. Magn. Reson.* **2011**, *212*, 204-215; b) M. Feike, D. E. Demco, R. Graf, J. Gottwald, S. Hafner, H. W. Spiess, *J. Magn. Reson., Ser A* **1996**, *122*, 214-221; c) W. Sommer, J. Gottwald, D. E. Demco, H. W. Spiess, *J. Magn. Reson., Ser A* **1995**, *113*, 131-134; d) I. Schnell, A. Lupulescu, S. Hafner, D. E. Demco, H. W. Spiess, *J. Magn. Reson.* **1998**, *133*, 61-69.

[95] K. Maruyoshi, D. Iuga, O. N. Antzutkin, A. Alhalaweh, S. P. Velagad, S. P. Brown, *Chem. Commun.* **2012**, *48*, 10844-10846.

[96] R. C. Zhang, Y. L. Hong, T. Ravula, Y. Nishiyama, A. Ramamoorthy, *J. Magn. Reson.* **2020**, *313*, 106717.

[97] a) E. Bartalucci, A. A. Malär, A. Mehnert, J. B. Kleine Büning, L. Günzel, M. Icker, M. Börner, C. Wiebeler, B. H. Meier, S. Grimme, B. Kersting, T. Wiegand, *Angew. Chem. Int. Ed.* **2023**, *62*, e202217725; *Angew. Chem.* **2023**, *135*, e202217725; b) J. Struppe, C. M. Quinn, S. Sarkar, A. M. Gronenborn, T. Polenova, *Mol. Pharm.* **2020**, *17*, 674-682.

[98] F. Fischer, S. Greiser, D. Pfeifer, C. Jager, K. Rademann, F. Emmerling, *Angew. Chem. Int. Ed.* **2016**, *55*, 14279-14283; *Angew. Chem.* **2016**, *128*, 14493-14497.

[99] T. X. Métro, C. Gervais, A. Martinez, C. Bonhomme, D. Laurencin, *Angew. Chem. Int. Ed.* **2017**, *56*, 6680-6680; *Angew. Chem.* **2017**, *129*, 6907-6911.

[100] C. H. Chen, I. Goldberga, P. Gaveau, S. Mittelette, J. Špačková, C. Mullen, I. Petit, T. X. Métro, B. Alonso, C. Gervais, D. Laurencin, *Magn. Reson. Chem.* **2021**, *59*, 975-990.

[101] B. Chen, X. Zhang, F. Wang, *Acc. Mater. Res.* **2021**, *2*, 364-373.

[102] S. D. Huo, P. K. Zhao, Z. Y. Shi, M. C. Zou, X. T. Yang, E. Warszawik, M. Loznik, R. Göstl, A. Herrmann, *Nat. Chem.* **2021**, *13*.